nature microbiology

Article

https://doi.org/10.1038/s41564-023-01368-0

Cryo-EM structure of the bacterial divisome core complex and antibiotic target FtsWIQBL

Received: 6 January 2023

Accepted: 23 March 2023

Published online: 1 May 2023

Check for updates

Lisa Käshammer[1,2], Fusinita van den Ent[1,2], Magnus Jeffery[1], Nicolas L. Jean[1], Victoria L. Hale[1] & Jan Löwe[1]

In most bacteria, cell division relies on the synthesis of new cell wall material by the multiprotein divisome complex. Thus, at the core of the divisome are the transglycosylase FtsW, which synthesises peptidoglycan strands from its substrate Lipid II, and the transpeptidase FtsI that cross-links these strands to form a mesh, shaping and protecting the bacterial cell. The FtsQ–FtsB–FtsL trimeric complex interacts with the FtsWI complex and is involved in regulating its enzymatic activities; however, the structure of this pentameric complex is unknown. Here, we present the cryogenic electron microscopy structure of the FtsWIQBL complex from *Pseudomonas aeruginosa* at 3.7 Å resolution. Our work reveals intricate structural details, including an extended coiled coil formed by FtsL and FtsB and the periplasmic interaction site between FtsL and FtsI. Our structure explains the consequences of previously reported mutations and we postulate a possible activation mechanism involving a large conformational change in the periplasmic domain. As FtsWIQBL is central to the divisome, our structure is foundational for the design of future experiments elucidating the precise mechanism of bacterial cell division, an important antibiotic target.

Cell division, or cytokinesis, is a fundamental process of life and, in most bacteria, is driven by peptidoglycan synthesis at the septum[1]. It is catalysed by the divisome, a multi-protein complex with more than 20 components that spans the cell envelope in bacteria harbouring a cell wall[2].

Central to the divisome is the peptidoglycan-synthesising protein complex FtsWI, with the transglycosylase (TG) FtsW polymerizing glycan strands from its substrate Lipid II[3,4], and the transpeptidase (TP) FtsI cross-linking peptide stems, thus forming a covalent mesh between glycan strands[5,6] (Fig. 1a). Septal peptidoglycan synthesis occurs after activation of the divisome glycosyltransferase-transpeptidase pair FtsWI[3], in particular through an interaction with the heterotrimer FtsQBL, as shown in vitro[7].

In this study, we present the cryogenic electron microscopy (cryo-EM) structure of the catalytic divisome core complex FtsWIQBL from *Pseudomonas aeruginosa* at a 3.7 Å resolution. The structure reveals details of the periplasmic interfaces within FtsWIQBL, including the positioning of FtsI by the coiled coil (CC) of FtsBL, as well as a transmembrane (TM) domain containing FtsWIBL but not FtsQ. With our structure, we can provide explanations of a multitude of known mutations that interfere with divisome activation and regulation. Finally, we suggest the existence of a large conformational switch between presumably the inactive and active states of the FtsWI core enzymes.

Our work is foundational for further structural, biochemical and genetic studies elucidating the molecular mechanisms of bacterial cell division. Because the divisome peptidoglycan synthase is essential for cell division in most bacteria, and is absent in eukaryotic cells entirely, it is a key target of important existing antibiotics and new antibiotic development[8]. Our structure will help to accelerate these efforts.

Cryo-EM structure of the core divisome complex FtsWIQBL

To solve the structure of the core divisome complex, we initially purified the *Escherichia coli* FtsWIQBL (*Ec*FtsWIQBL) complex expressed in insect cells (Extended Data Fig. 1a). Several approaches, including

[1]Medical Research Council Laboratory of Molecular Biology, Cambridge, UK. [2]These authors contributed equally: Lisa Käshammer, Fusinita van den Ent. e-mail: jyl@mrc-lmb.cam.ac.uk

https://doi.org/10.1038/s41564-023-01368-0

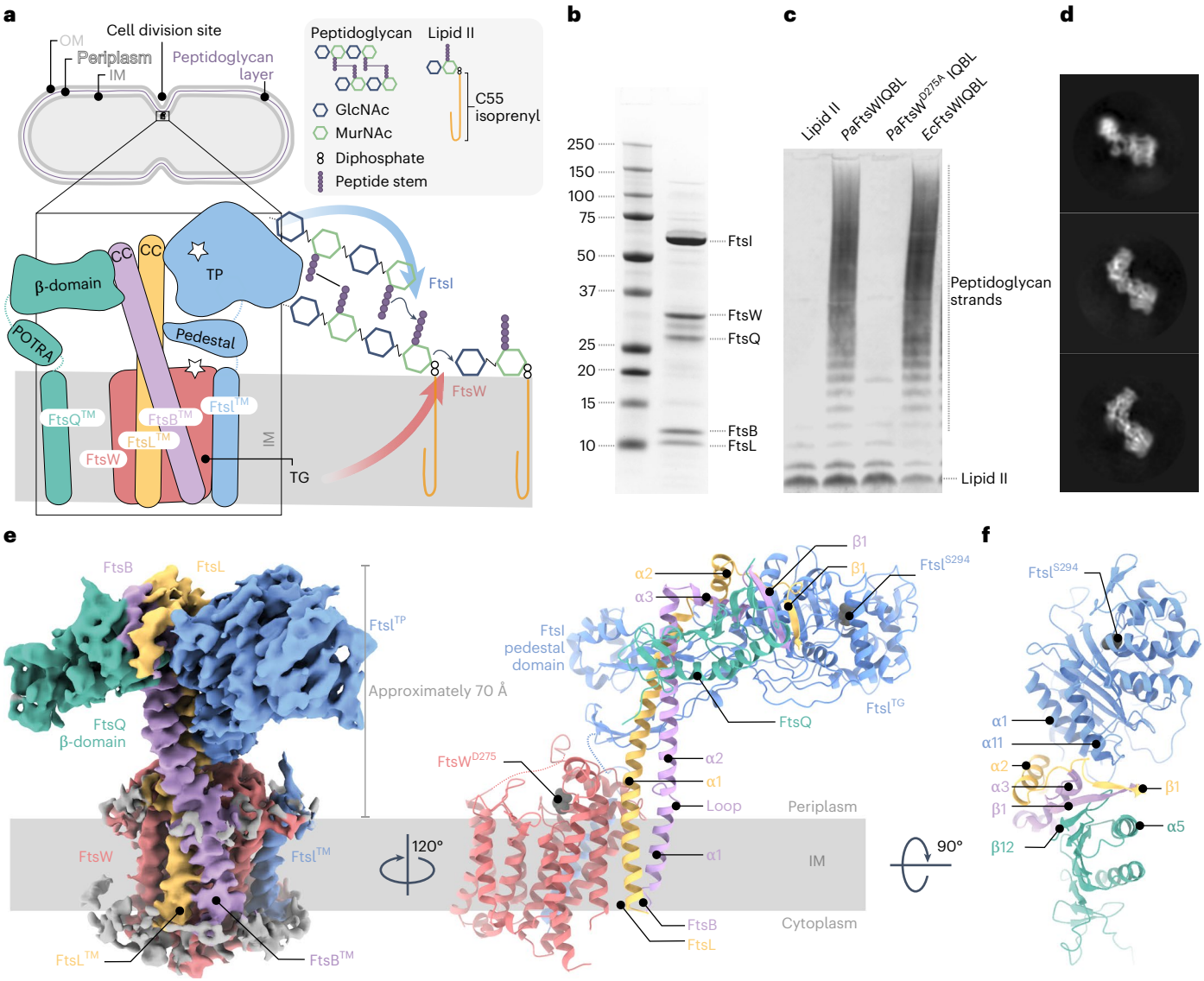

Fig. 1 | Biochemical and structural characterization of the core divisome complex FtsWIQBL from *P. aeruginosa*. **a**, Septal peptidoglycan synthesis by FtsWIQBL during Gram-negative bacterial cell division. The TG FtsW (red) and TP FtsI (blue) bind the non-enzymatic subcomplex FtsQBL (green, violet and yellow, respectively). The complex contains 14 TM helices: ten from FtsW and one each from FtsIQBL. The TG FtsW catalyses the polymerization of *N*-acetylglucosamine (GlcNAc)-*N*-acetylmuramic acid (MurNAc) disaccharides from Lipid II. The TP FtsI cross-links the peptides from the nascent chain to adjacent peptides in the peptidoglycan layer between residues three and four. IM, inner membrane; OM, outer membrane. **b**, SDS–polyacrylamide gel electrophoresis (PAGE) of the copurified *Pa*FtsWIQBL complex after size-exclusion chromatography (SEC). **c**, Western blot showing glycan strand ladders synthesized by divisome core complexes from Lipid II, demonstrating TG activity. The negative control does not contain any FtsWIQBL (lane 1). Wild-type *P. aeruginosa* and *E. coli* FtsWIQBL complexes (lanes 2 and 4) are active TGs, while the *P. aeruginosa* putative active site mutant FtsW^{D275A}IQBL (lane 3) is inactive. **d**, Three representative 2D classes from our *Pa*FtsWIQBL cryo-EM data. **e**, Left, side-view of the *Pa*FtsWIQBL cryo-EM density at an overall resolution of 3.7 Å. Protein colours are the same as those in **a**. Residual density from the detergent micelle is visible around the TM domain and is shown in grey. Right, model of *Pa*FtsWIQBL, rotated by 120° with respect to the density on the left-hand side. The putative FtsW active site residue D275 is indicated, as is the FtsI active site residue S294. FtsW loop 219–233 and FtsI loop 45–50 are shown as dotted lines because they were too flexible to build. FtsQ^{TM} and FtsQ$^{\beta}$ were not resolved and are not shown. **f**, Top view of the periplasmic domain, showing interactions between FtsI, FtsL, FtsB and FtsQ.

detergents, amphipols and reconstitution in nanodiscs were used in attempts to obtain a high-resolution *Ec*FtsWIQBL structure. The best cryo-EM results of the *Ec*FtsWIQBL sample were achieved in nanodiscs (Extended Data Fig. 1b–d); however, due to variability in the obtained nanodisc size and composition, as well as strong alignment on the nanodisc during processing, we were unable to solve the *Ec*FtsWIQBL structure. Therefore, we switched to the *Pseudomonas aeruginosa* FtsWIQBL (*Pa*FtsWIQBL) complex expressed in *E. coli* (Fig. 1b and Extended Data Fig. 1e). Both *Ec*FtsWIQBL and *Pa*FtsWIQBL possess comparable TG activity, while the putative active site mutant *Pa*FtsW^{D275A}IQBL is inactive (Fig. 1c). This is in accordance with previous data where the *Pa*FtsW^{D275A}IQBL mutant displayed reduced TG activity in vitro and caused filamentation in *P. aeruginosa* cells when overexpressed[3]. Having confirmed that our purified *Pa*FtsWIQBL complex produced peptidoglycan strands, we proceeded with single-particle averaging cryo-EM and determined the structure of *Pa*FtsWIQBL to a final overall resolution of 3.7 Å (Fig. 1d,e, Extended Data Figs. 1f, 2 and 3, and Supplementary Table 1).

General architecture of the FtsWIQBL complex

All five proteins were resolved in the final cryo-EM reconstruction (Fig. 1e), with FtsQ being partially disordered. The density for the

membrane domain of *Pa*FtsWIQBL revealed 13 TM helices, including ten helices from FtsW, plus one each from FtsI, FtsB and FtsL (Extended Data Fig. 4a). Density for the FtsQ TM helix ($FtsQ^{TM}$) was not observed (Extended Data Fig. 4b). The detergent micelle density was subtracted from the final reconstruction and the position of the complex in the membrane was approximated using the Orientations of Proteins in Membranes webserver[9] (Fig. 1e and Extended Data Fig. 4b,c).

The periplasmic domains of the *Pa*FtsWIQBL complex extend about 70 Å away from the membrane in a 'Y' shape, with the FtsI TP domain ($FtsI^{TP}$) and the FtsQ β-domain ($FtsQ^{\beta}$) located on opposite arms of the Y, and FtsBL connecting them (Fig. 1e,f). Interestingly, only $FtsQ^{\beta}$ is well resolved, while the density for the FtsQ polypeptide transport-associated domain (POTRA) ($FtsQ^{POTRA}$) is only visible in low-resolution maps at high contour level, and the density for $FtsQ^{TM}$ is completely absent (Extended Data Fig. 4d). $FtsQ^{POTRA}$ adopts a slightly different orientation relative to $FtsQ^{\beta}$ compared to previously determined X-ray structures[10–12] (Extended Data Fig. 4d). Taken together, this shows that FtsQ is tethered to FtsWILB via its $FtsQ^{\beta}$-FtsB interaction, while $FtsQ^{POTRA}$ and $FtsQ^{TM}$ are flexibly attached in the current complex (Fig. 1f). Because $FtsQ^{TM}$ is not visible, we assume it is not in the micelle that contains the other TM segments but might be surrounded by detergent molecules separately. While it has been previously reported that FtsB dimerizes and could thus facilitate the dimerization of core divisome components[13,14], we found no evidence for higher oligomeric species in our cryo-EM data. We cannot exclude dimerization of FtsB on its own; however, in our current structure, dimerization via FtsB would be hindered by the presence of FtsI or FtsQ.

FtsL and FtsB have similar folds, each consisting of a long α-helical CC segment, followed by a short α-helix and a β-strand. Interestingly, the FtsB α-helical CC is interrupted by a small, conserved loop just above $FtsB^{TM}$ that might aid with sterically maintaining the correct insertion depth in the membrane (Figs. 1e and 2a). The observed interruption of the FtsB CC was postulated previously using computational models[14,15]. FtsB and FtsL interact with each other over their entire lengths through mainly hydrophobic interactions, for example, between $FtsL^{\alpha1}$ and $FtsB^{\alpha2}$ (Fig. 2a and Extended Data Fig. 5a). Thus, our structure clarifies the FtsL-FtsB interaction and confirms previous reports that suggested a CC interaction between FtsB and FtsL[16,17].

The TG FtsW and TP FtsI share two interfaces. The first interface is in the membrane, where $FtsI^{TM}$ interacts with the TM8 and TM9 of FtsW (Extended Data Fig. 4a), an interaction that closely resembles that of the previously reported RodA-PBP2 elongasome complex from *Thermus thermophilus*[18]. The second interaction site is located between the extracellular loop 4 of FtsW ($FtsW^{EC4}$) and the linker between $FtsI^{TM}$ and $FtsI^{Pedestal}$. Due to the flexibility of FtsI in this region, not all contacts could be determined unambiguously.

The cytoplasmic tail of *E. coli* FtsL is required for the recruitment of FtsW[19]. In the structure presented in this study, the FtsL cytoplasmic tail could not be traced unambiguously. This could either point towards a transient interaction during recruitment or species-specific differences in recruitment due to the size of the cytoplasmic tail (11 residues in *P. aeruginosa* versus 34 residues in *E. coli*). However, we clearly observed FtsL-FtsW interactions in the periplasm ($FtsW^{EC1}$ and $FtsL^{\alpha1}$), and within the membrane through $FtsW^{TM1}$ and the upper three turns of $FtsL^{TM}$. In the latter, the lower part of $FtsL^{TM}$ twists away from FtsW because of its gyrating CC interaction with FtsB (Extended Data Fig. 5b).

FtsIQBL interactions in the periplasm

FtsL and FtsI form an extensive interface in the periplasm, with a total buried surface area of 1,035 $Å^2$. The FtsL-FtsI interaction is facilitated by two sites: $FtsL^{\alpha1}$-$FtsI^{Pedestal}$, involving the anchor and head subdomain residues in $FtsI^{Pedestal}$ and $FtsL^{\alpha2,\beta1}$-$FtsI^{TP}$ (Fig. 2b and Extended Data Fig. 5c). Moving along the FtsL coil, the first mainly hydrophobic and neutral interactions occur between $FtsL^{\alpha1}$ (residues L41–L48) and the anchor subdomain of $FtsI^{Pedestal}$ (residues I58, R193, Q208–Q215; Fig. 2b, panel 1). $FtsI^{Pedestal}$ slightly wraps around $FtsL^{\alpha1}$, forming a hydrophilic interaction site ($FtsI^{H61}$ with $FtsL^{R51}$, $FtsL^{D52}$ and $FtsL^{Q55}$; Fig. 2b, panel 2). The final and mainly hydrophobic interaction site on $FtsL^{\alpha1}$ involves residues A56–S66 and residues located mainly in the $FtsI^{Pedestal}$ head subdomain (L64, P72–P78, F151–P156; Fig. 2b, panel 2). Importantly, no direct interaction was observed between the FtsB CC and FtsI (Fig. 2b and Extended Data Fig. 5a).

The second FtsL-FtsI interaction site is located on top of the periplasmic domain (Fig. 2b, panel 3): $FtsL^{\alpha2,\beta1}$-$FtsI^{TP}$. H71 of $FtsL^{\alpha2}$ stacks against Y229 of $FtsI^{TP}$ and is flanked by additional residues in FtsB (E79, L80), FtsI (R233) and FtsL (E75). An additional hydrophobic interface site is formed by several proline residues in both FtsL and $FtsI^{TP}$ (P556, P557 (FtsI) – M94 (FtsL); P557, G478, P477 (FtsI) – P89 (FtsL); R551 (FtsI) – P87 (FtsL)). Interestingly, $FtsB^{\alpha3}$ and $FtsB^{\beta1}$ frame a loop in FtsQ between the β-strands 11 and 12, forming the only interaction site between FtsI, FtsB and FtsQ (N554 (FtsI) – N265 (FtsQ) – Q91 (FtsB); R226 (FtsI) – P264 (FtsQ); R226 (FtsI) – H78 (FtsB, backbone), R551 (FtsI) – L80 (FtsB, backbone)). FtsI adopts a structure very similar to previously reported crystal structures[20], with only minor changes in the $FtsI^{Pedestal}$ domain, indicating that FtsL binding does not cause large rearrangements in $FtsI^{TP}$ (Extended Data Fig. 6a).

Only a few FtsL-FtsQ contacts are present; however, FtsL completes an extended β-sheet formed between the $FtsQ^{\beta}$ strands β5 to β12 and $FtsB^{\beta1}$, by contributing its last β-strand (Fig. 1f and Fig. 2b, panel 3). The FtsB-FtsQ interaction recapitulates that of previously determined crystal structures, where only small parts of $FtsB^{11,12}$ were resolved (Extended Data Fig. 6b). In addition, the cryo-EM structure shows an interaction between the $FtsB^{\alpha2}$ (starting from E53) and $FtsQ^{\beta}$ loops (R183, S212–R214, R231). Interruption of the FtsB-Q interface with inhibitors based on the minimal interface could be expected to also disrupt the interface in the context of the divisome core complex[21].

Comparison with RodA–PBP2 structures and AlphaFold 2 predictions

Cell elongation in rod-shaped bacteria is facilitated by the elongasome that, like the divisome, polymerizes and cross-links peptidoglycan, but is positioned throughout the cell envelope by moving MreB filaments[22]. RodA, the elongasome's TG is related to FtsW and has previously been structurally characterized using X-ray crystallography both on its own and as a RodA–PBP2 complex[18,23] (the latter being homologous to FtsWI). The structures of *Pa*FtsW determined in this study and *Tt*RodA are very similar, with the exception of TM7, which appears to be somewhat flexible in the cryo-EM structure, straighter with respect to that of *Tt*RodA and closer to TM5 than in *Tt*RodA–PBP2 (Extended Data Fig. 6c). It has been postulated that the movement of TM7 could open a cavity for the binding of the lipid tail of Lipid II to RodA[18] and the location of TM7 in *Pa*FtsWIQBL creates such a cavity. The putative catalytic residue D275 is located in a deep, highly conserved cleft, as shown in Extended Data Fig. 6d, which we suggest might harbour the sugar moieties of Lipid II during the TG reaction.

The most striking observation when comparing *Pa*FtsWIQBL with *Tt*RodA–PBP2 is the difference in the relative orientations of the TP with respect to the TG domain, despite the fact that the structures of the single proteins superimpose well on their own. Alignment of both complexes on the FtsW/RodA subunits places $PaFtsI^{TP}$ and $TtPBP2^{TP}$ almost opposite to each other, requiring an approximate 130° rotation of $PaFtsI^{TP}$/$TtPBP2^{TP}$ for their interconversion (Extended Data Fig. 7a,b). The reason for this large difference is unclear but is possibly caused by the presence of FtsQBL in our divisome structure and the absence of binding partners such as MreCD in the elongasome structure. Alternatively, the differences could be intrinsic to the elongasome and divisome complexes or reflect different, distinct states in the regulatory and catalytic cycles of the enzyme complexes.

We used AlphaFold 2 multimer[24] (AF2) to predict *Pa*FtsWIQBL; many of the large-scale and fine features observed in the *Pa*FtsWIQBL

https://doi.org/10.1038/s41564-023-01368-0

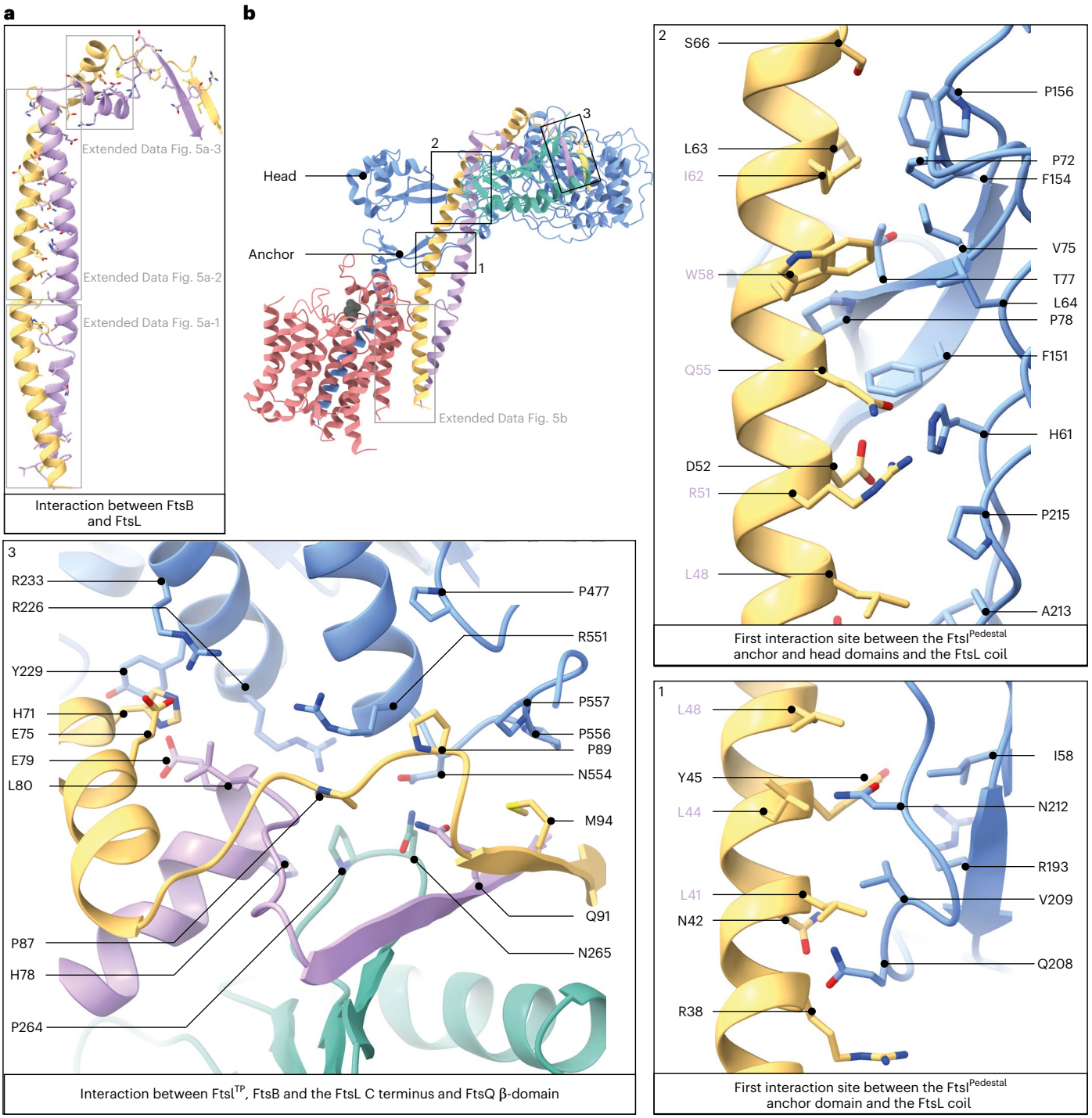

Fig. 2 | Interactions between FtsI, FtsQ, FtsB and FtsL. a, FtsB and FtsL adopt similar folding and interact with each other over their whole length. The boxes with the grey outline indicate regions that are further discussed in Extended Data Fig. 5a. **b**, Key interactions within the FtsWIQBL periplasmic domain are highlighted in boxes 1–3. The box with the grey outline indicates a region that is further discussed in Extended Data Fig. 5b. The interactions between FtsI^{Pedestal} and the FtsL CC are shown in panels 1 and 2. Most residues at the interface between FtsI and FtsL in this region are hydrophobic or neutral. Residues in FtsL that also face FtsB are highlighted in violet. The interaction between FtsI, FtsL, FtsB and FtsQ as seen from the top of the periplasmic domain is shown in panel 3.

structure were predicted correctly by AF2, including the lack of an interaction between the membrane-embedded FtsQ^{TM} and FtsWIBL^{TM}. However, in the AF2 model the periplasmic FtsIQBL interaction site is rotated upwards by about 30°, moving FtsI^{TP} closer towards where the peptidoglycan layer is located (Extended Data Fig. 7a,c). Furthermore, a small rearrangement in the anchor subdomain FtsI^{Pedestal}-FtsL^{α1} shifts the interacting residues on FtsI^{Pedestal} from 208–212 to 203–206. To understand the implications of these differences, both structures were fitted into a to-scale model of the cell envelope of *E. coli*, produced from a cellular electron cryotomogram (Fig. 3a). Using the cryo-EM structure, the active site of FtsI^{TP} does not reach the peptidoglycan layer but does so in the more extended AF2 model. Because AF2 uses evolutionary couplings between amino acids[24], in addition to protein structural features that correlate with sequence, it more probably

https://doi.org/10.1038/s41564-023-01368-0

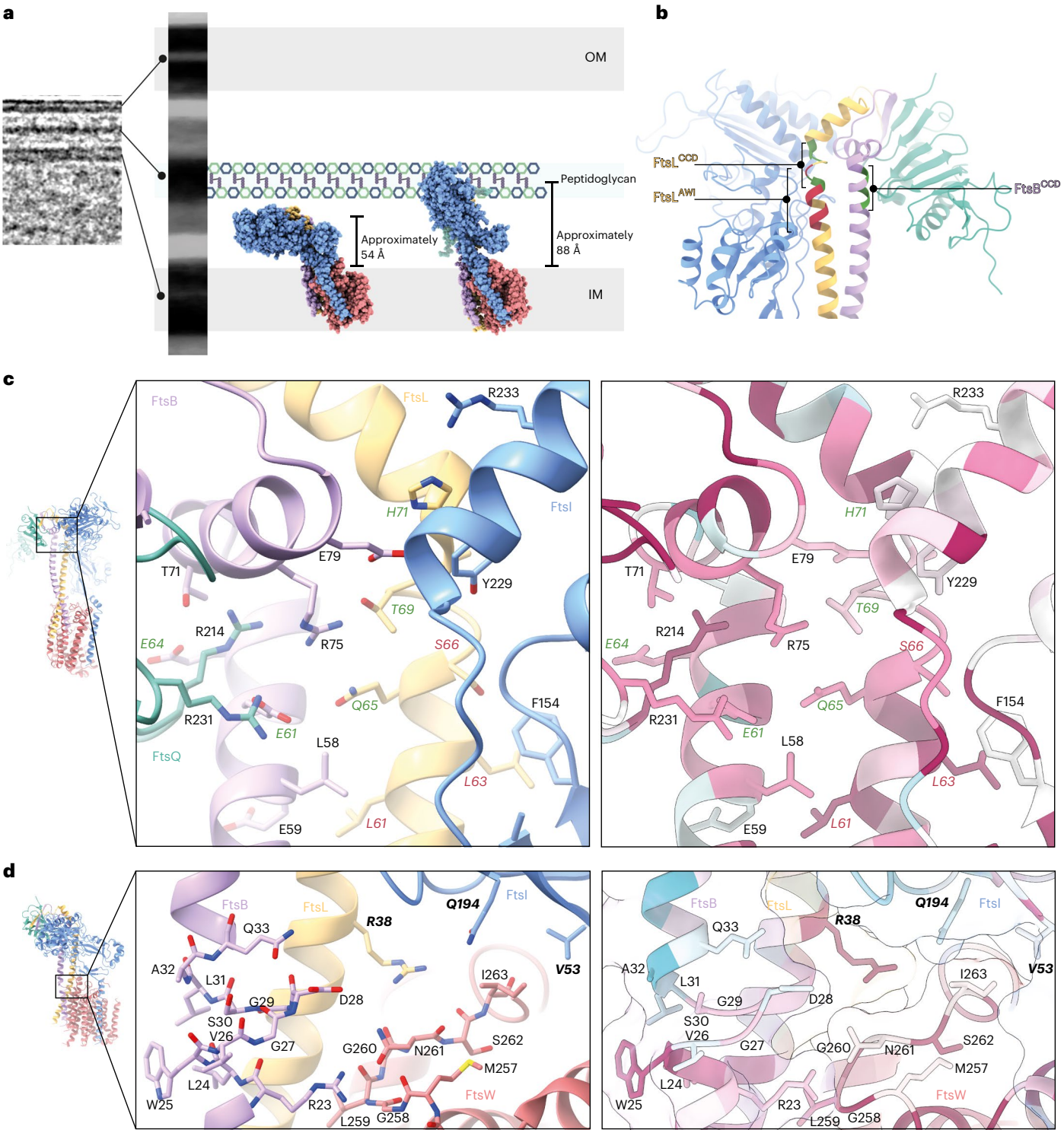

Fig. 3 | Interactions that affect divisome regulation. a, To-scale model of the *E. coli* cell envelope generated from a cellular electron cryotomogram. The cryo-EM FtsWIQBL atomic model (left) and the AF2 prediction (right) are docked into the IM. When placing both structures into the IM, the FtsI TP domain of our cryo-EM structure does not extend to the peptidoglycan layer, yet it does so in the AF2 structure. The measured distances of the active site residue FtsI^{S294} to the IM plane are indicated. **b**, The C termini of the FtsB and FtsL CCs with the CCD (green) and AWI (red) regions are highlighted, showing the FtsB^{CCD} facing FtsQ and FtsL^{AWI} facing FtsI. **c**, Region around the activating mutations FtsL^{Q65} (E88 in *E. coli*) and FtsB^{E61} (E56 in *E. coli*). Residues with known divisome activating mutations, which lead to smaller cells, are shown in green. Residues with known LOF mutations, which cause a defect in cell division, are shown in red. Sequence conservation analysis (calculated with ConSurf[61]) showed a high degree of conservation for many residues in this area. **d**, Residues surrounding the region of discontinuity in the FtsB CC. This region contains residues with known LOF mutations (shown in bold). Many residues in this region are highly conserved, including FtsL^{R38} (R61 in *E. coli*), which inserts between FtsI and FtsW and is located close to a highly conserved loop in FtsW (M257–I263, Q279–V285 in *E. coli*), that is, in close proximity to the putative active site residue D275 (D297 in *E. coli*).

predicts the active state of FtsWIQBL that one would expect to be selected for during evolution. Thus, the cryo-EM structure and AF2 prediction may represent the inactive and active (catalytic) states of the divisome core complex, respectively. Because our sample shows TG activity in vitro and the cryo-EM structure is substrate-free (apo), it is at least theoretically possible that Lipid II substrate binding contributes to the interconversion of the two states. In addition, other factors such as FtsN or peptidoglycan chains might be required to achieve the proposed conformational change. Recently, a study on RodA–PBP2 reported a similar upswinging mechanism[25], which indicates that the concept of regulating the enzymatic activities via restricting access to the peptidoglycan layer might be conserved between the divisome and the elongasome. However, important differences exist between divisome and elongasome regarding the conformation before the upswinging motion and most probably also between the signals required to initiate this conformational change.

FtsN triggers constriction in cells[26,27]. It is the last protein to be recruited to the division site in *E. coli* and its recruitment is dependent on the presence of earlier divisome proteins, including FtsA, FtsQ and FtsI[26,28–30]. However, we have not been able to generate a biochemically stable *E. coli* FtsN–FtsWIQBL complex and previous studies reported that the addition of the FtsN periplasmic domain did not yield an increase in *P. aeruginosa* TG activity in vitro[7]. Whether FtsN activates the core divisome beyond the TG activity levels seen in this study through binding of FtsQLB, or whether the in vitro sample cannot be further activated will need further investigations including addition of other divisome components, for example, FtsA, FtsN or DedD, as well as the substrate Lipid II. It is also possible that FtsN is involved only in regulating TP activity.

Interactions that affect divisome regulation

The constriction control domain (CCD) of the divisome was identified previously from a set of mutations that allow partial or complete bypass of the requirement for FtsN in *E. coli*[31,32]. In our structure, these residues cluster at the top of FtsL$^{\alpha1}$ and FtsB$^{\alpha2}$, with the FtsB^{CCD} mutations facing FtsQ$^{\beta}$. Furthermore, in close proximity are the activation of FtsWI (AWI) residues on FtsL$^{\alpha1}$ that display a dominant negative phenotype when mutated[19] (Fig. 3b).

The CCD residues FtsB^{E61} (*Ec*E56G/A/K/V) and FtsL^{Q65} (*Ec*E88K/V) point towards a positively charged cavity formed by three arginine residues (FtsQ^{R214}, FtsQ^{R231}, FtsB^{R75}), flanked by FtsL^{T69} (*Ec*G92D, CCD residue) on one side and FtsB^{E64} (*Ec*D59H/V, CCD residue) and FtsB^{T71} on the other side. This interface contains many charged and conserved residues (Fig. 3c); removal of a charge or introduction of the opposite charge could well result in destabilization of the interface and potentially increased flexibility of the protein. This may allow FtsWIQBL to adopt an elongated and more active conformation more readily, as possibly indicated by the AF2 model, and with less or no activation signal, for example, from FtsN.

A dominant negative phenotype was previously reported for the AWI mutation *Ec*L86F[19]; its *P. aeruginosa* equivalent FtsL^{L63} interacts with FtsI^{F154} in FtsI^{Pedestal} (Fig. 3c). Replacing the leucine with the bulkier phenylalanine probably causes a steric clash that weakens the FtsI-FtsL interaction. FtsL^{S66} (*Ec*N89S, *Pa*S66D) was classified as a CCD mutation in *E. coli*[31] but has a dominant negative phenotype in *P. aeruginosa*, with reduced in vitro TG activity[7], probably due to a steric clash with FtsI^{F154}. Mutation of FtsL^{L61} (*Ec*L84K/D) has a dominant negative phenotype and affects FtsL localization to the septum[19,33], indicating that the integrity of the FtsBL CC interaction is vital for a functional complex, as well supported by our structure where the FtsBL CC is at the centre of the complex.

The AWI residue FtsL^{R38} (*Ec*R61E/C) is highly conserved and located between FtsW$^{M257–I263}$ and the anchor subdomain of FtsI^{Pedestal} (Fig. 3d). Mutation of this residue causes a dominant negative phenotype in both *E. coli* and *P. aeruginosa* and reduced in vitro TG activity in *P. aeruginosa*[7,19]. FtsL^{R38} might interact with the highly conserved FtsW^{G260} and FtsW^{S262} residues and stabilize FtsW$^{M257–I263}$ together with FtsB^{R23}, a hypothesis supported by the fact that the corresponding loop in RodA and RodA–PBP2 is disordered[18,23]. The aforementioned FtsB CC discontinuity, the C terminus of FtsB^{R23}, might be required to allow for some flexibility of FtsB during the catalytic cycle of FtsW. *Ec*FtsI^{L62P} and *Tt*PBP2^{L43R} correspond to *Pa*FtsI^{V53} and result in a strong cell division defect and reduced TG activity in vitro, respectively[18,34]. *Pa*FtsI^{V53} interacts with *Pa*FtsW^{I257} in our structure, bringing the linker between FtsI^{TM} and FtsI^{Pedestal} in close proximity to FtsW. Thus, FtsW$^{M257–I263}$ presents an interaction site for FtsL, FtsB and FtsI in close proximity to the putative FtsW active site.

The recruitment of FtsQ to midcell requires FtsK[10,29,35]. AF2 predicts that the interaction between FtsK$^{1–222}$ and FtsWIQBL occurs through FtsQ^{POTRA} β2 and α3; this interaction is also identified by coevolutionary coupling analysis using EVcouplings[36] as an FtsQ–FtsK complex interaction hotspot (6 of 10 couplings; Extended Data Fig. 8a,b). Residues previously identified as impairing FtsK recruitment when mutated[10] (*Ec*Q108, *Ec*V92, *Ec*V111, *Ec*K113) map onto this conserved region (Extended Data Fig. 8c). We copurified an FtsQK$^{1–222}$ complex using *E. coli* proteins, which confirmed that the two proteins interact tightly and constitutively (Extended Data Fig. 8d). To further our understanding of divisome recruitment and regulation, in the future larger divisome complexes will need to be assembled. For example, divisome interactions with FtsA, through FtsN, FtsK and possibly FtsQ have the potential to modify the conformations, oligomeric states and activities of the core complex and its enzymes.

We report the structure of the essential bacterial cell division complex and important future antibiotic target FtsWIQBL from *P. aeruginosa* and show that *Pa*FtsWIQBL forms a stable Y-shaped complex that harbours intrinsic TG activity. Our *Pa*FtsWIQBL structure explains many subunit contacts that have previously been shown to be important through loss-of-function (LOF) and bypass mutations. In addition, an AF2 model revealed a different, probably catalytically competent state that allows for peptidoglycan cross-linking by FtsI. While our analysis hints at the nature of the catalytic state, further research is needed to resolve more states and their associated conformational changes, which possibly requires the addition of activating proteins such as FtsA or FtsN (or both) as well as the substrate Lipid II and its derivatives or products as ligands. It will be particularly exciting to resolve the enzymatic mechanism of the FtsW TG because it is a promising drug target for new antibiotics given its function, conservation, periplasmic accessibility and very wide phylogenetic distribution. To gain a deeper understanding of the mechanism of the divisome, the inclusion of upstream and downstream proteins, for example, FtsEX, FtsK, PBP1b and DamX will also be necessary. Our work is an important milestone in the 25-year quest for a molecular understanding of the ancient, near ubiquitous and medically important process of FtsZ-based bacterial cell division.

Methods

Cloning

The primers used for the Gibson assembly are listed in Supplementary Table 2. The generated expression plasmids are listed in Supplementary Table 3. All constructs were confirmed by sequencing.

*Pa*FtsWIQBL

Cloning, expression and purification of *Pa*FtsWIQBL (UniProt IDs: Q9HW00 (FtsW), G3XD46 (FtsI), G3XDA7 (FtsQ), Q9HVZ6 (FtsL) and Q9HXZ6 (FtsB)) were adapted from a previously published protocol[7] with some changes, including the switch from a FLAG-tag to a Strep-tag.

*Ec*FtsWIQBL

The *Ec*FtsWIQBL complex (UniProt IDs: P0ABG4 (FtsW), P0AD68 (FtsI), P06136 (FtsQ), P0AEN4 (FtsL), P0A6S5 (FtsB)) was expressed in insect

cells through a single baculovirus vector, which was assembled using the biGBac system[37]. To increase expression levels of FtsL, the mutations S3N, R4K and V5L were introduced[38]. Additionally, to ensure equal expression levels, a fusion of FtsW and FtsI, as found naturally in some organisms (Supplementary Table 4), was created with a GSGASG cytoplasmic linker between the FtsW C terminus and the FtsI N terminus.

E. coli FtsQK$^{1-122}$

Genes encoding FtsQ-His$_6$ (UniProt ID: P06136) and Twin-Strep-FtsK$^{1-222}$ (UniProt ID: P46889) were ordered as gBlocks (Integrated DNA Technologies) and cloned into pLIB. The gene expression cassettes were amplified and inserted into pBIG1a[37] forming pNJ069.

Baculovirus generation

Baculoviruses containing pFE758 and pNJ069 were used for insect cell expression of *Ec*FtsWIQBL and *E. coli* FtsQK$^{1-122}$ (*Ec*FtsQK$^{1-122}$), respectively. The recombinant baculoviral genomes were generated by TN7 transposition in DH10bacY cells[39]; this bacmid was used to transfect Sf9 cells (Thermo Fisher Scientific) using FuGENE (Promega Corporation). After 3–5 d, the culture was centrifuged and the virus-containing supernatant was collected and stored in the presence of 1% FCS.

Bacterial expression

*Pa*FtsWIQBL was expressed in *E. coli*. pLK1, pLK2 and pLK3 were sequentially transformed into *E. coli* C43(DE3) cells. A total of 120 ml of overnight culture were added to 12 l terrific broth medium with 2 mM $MgCl_2$, kanamycin (25 μg ml^{-1}), chloramphenicol (25 μg ml^{-1}) and ampicillin (50 μg ml^{-1}), and grown at 37 °C to an OD_{600} of 0.7. Protein expression was induced with 1 mM isopropylthio-β-galactoside and 1 g arabinose per litre and continued at 18 °C overnight. Cells were collected by centrifugation for 20 min at 4,000*g* at 4 °C, flash-frozen in liquid nitrogen and stored at −80 °C.

Insect cell expression of *Ec*FtsWIQBL and *Ec*FtsQK$^{1-222}$

Sf9 cells were grown in Insect-XPRESS medium (Lonza) to a density of 1.5–2 million cells per millilitre, infected with approximately 1% amplified baculovirus and collected by centrifugation after 60–70 h, when cell viability reached approximately 80%. Cell pellets were washed with PBS, flash-frozen in liquid nitrogen and stored at −80 °C.

Protein purifications

All purifications, including the centrifugation steps, were performed at 4 °C. Proteins were aliquoted, flash-frozen in liquid nitrogen and stored at −80 °C, except when cryo-EM grids were directly prepared from freshly eluted protein. For the activity assay (see below), protein concentration was determined using the Protein Assay dye reagent concentrate (Bio-Rad Laboratories).

*Pa*FtsWIQBL

Cells from 12 l of *E. coli* culture were resuspended in a final volume of 300 ml lysis buffer (20 mM HEPES, 150 mM NaCl, 20 mM $MgCl_2$, pH 7.5, 1 mM dithiothreitol) containing DNase (Sigma-Aldrich) and RNase (Sigma-Aldrich) and twice passed through a cell disruptor (Constant Systems) at 25,000 pounds per square inch (psi). The lysate was centrifuged for 1 h at 234,998*g* (Type 45 Ti rotor; Beckman Coulter). Membranes were homogenized using a Dounce tissue grinder (Whaeton) in solubilization buffer (20 mM HEPES, 500 mM NaCl, 20% glycerol, pH 7.0). Membrane-bound proteins were solubilized with lauryl maltose neopentyl glycol (LMNG) detergent (Anatrace) at a final concentration of 1% (w/v) and rotated for at least 1 h. The volume was doubled with solubilization buffer; 12 μl benzonase (Merck) were added. The solution was centrifuged for 1 h at 234,998*g* and the supernatant was bound to 2 ml (CV) of equilibrated Strep XT4 Flow beads (IBA Lifesciences) while rotating for 2 h. Beads were collected in a column and washed with 50 ml of wash buffer 1 (solubilization buffer plus 0.1% LMNG) and 50 ml of wash buffer 2 (solubilization buffer plus 0.01% LMNG). Protein was eluted from the Strep beads over 10 CV in 2-ml fractions with elution buffer (20 mM HEPES, 500 mM NaCl, 20% glycerol, 50 mM biotin, pH 7.0, 0.005% LMNG). All elution fractions were pooled and concentrated to 50 μl using 100-kDa centrifugal concentrators (Vivaspin). The concentrated sample was further purified using a Superose 6 Increase 3.2/300 size-exclusion column (Cytiva), equilibrated in size-exclusion buffer (20 mM HEPES, 300 mM NaCl, pH 7.0, 0.005% LMNG).

*Ec*FtsWIQBL

Sf9 cells were resuspended in lysis buffer (20 mM HEPES, pH 8.0, 500 mM NaCl, 10% glycerol, 2 mM tris(2-carboxyethyl)phosphine (TCEP)), containing 1 mM phenylmethylsulfonyl fluoride (PMSF), protease inhibitor tablets (cOmplete EDTA-free Protease Inhibitor (Roche), 1 per 25 ml), DNase and RNase, and sonicated for 2 min (1 s pulse on, 10 s pulse off, 70% intensity), after which 2 mM EDTA was added. The lysate was centrifuged for 1 h at 235,000*g*. The pellet was homogenized using a Dounce tissue grinder in solubilization buffer (20 mM HEPES, pH 8.0, 10 mM $MgCl_2$, 500 mM NaCl, 20% glycerol) containing 1 mM PMSF and protease inhibitor tablets. Detergent glyco-diosgenin (GDN) (Anatrace) was added to a final concentration of 1% to solubilize the membrane-bound proteins and rotated for 2 h, before centrifugation to remove nuclei (10 min, 3,200*g*). The supernatant was diluted fivefold with Strep buffer (20 mM HEPES, pH 8.0, 350 mM NaCl, 10% glycerol, 1 mM TCEP) in the presence of benzonase; the NaCl concentration was reduced to 350 mM before centrifuging for 45 min at 142,000*g*. The supernatant was cycled over a 5-ml StrepTrap HP column (Cytiva) overnight. The StrepTrap HP column was washed with 50 column volumes of Strep buffer including 0.01% GDN at 5 ml min^{-1}. The protein complex was eluted in Strep buffer supplemented with 2.5 mM desthiobiotin (Sigma-Aldrich) at 1 ml min^{-1}. Fractions containing the complex were pooled and concentrated to 50 μl using 100-kDa centrifugal concentrators and further purified using a Superose 6 Increase 3.2/300 size-exclusion column in SEC buffer (20 mM HEPES, pH 8.0, 350 mM NaCl, 10% glycerol, 1 mM TCEP, 0.01% GDN).

*Ec*FtsWIQBL reconstitution in nanodiscs for cryo-EM

The Nano Quick protocol[40] was adapted to reconstitute the complex into nanodiscs. Proteins were expressed and the membrane was solubilized as described above; however, instead of GDN, a mixture of LMNG:cholesteryl hemisuccinate (CHS) (10:1) was used at a final concentration of 1%. The solubilized protein was incubated overnight with StrepTactin sepharose beads (Cytiva). The beads were washed in Strep buffer including 0.1% LMNG:CHS (10:1) and then into SEC buffer including 2% glycerol and 0.1 % LMNG:CHS (10:1). A 1,000-fold molar excess of 1-palmitoyl-2-oleoyl-sn-glycero-3-phosphoglycerol (POPG) was added and incubated for 1 h, followed by a 20-fold excess of membrane scaffold protein 2N2 (purified as described in Ritchie et al.[41]). After 15 min, activated Bio-Beads SM-2 (Bio-Rad Laboratories) were added and the mixture was rotated overnight. The protein complex was eluted in Strep buffer supplemented with 2.5 mM desthiobiotin and subjected to SEC as above in SEC buffer without detergent.

*Ec*FtsQK

Cells from 1 l of culture were resuspended in 50 ml lysis buffer (50 mM Tris, 500 mM NaCl, pH 8.0) supplemented with DNase, RNase and protease inhibitor tablets (1 per 25 ml) and sonicated for 2 min (1 s on, 10 s off, 70% intensity). The lysate was centrifuged for 25 min at 25,000*g* (25.50 rotor; Beckman Coulter); the supernatant was subsequently centrifuged for 1 h at 200,000*g* (Ti 45 rotor; Beckman Coulter). The membranes were homogenized with a Dounce homogenizer and solubilized in 35 ml solubilization buffer (50 mM Tris, 350 mM NaCl, pH 8.0, 1% GDN, 10% glycerol) for 2 h. The solution was diluted to 50 ml with dilution buffer (50 mM Tris, 350 mM NaCl, pH 8.0, 10% glycerol) and centrifuged for 30 min at 80,000*g* (Ti 75 rotor; Beckman Coulter).

The supernatant was diluted to 500 ml with dilution buffer and cycled overnight over a 1-ml StrepTrap HP column. The column was washed with 70 ml of buffer A1 (50 mM Tris, 350 mM NaCl, 0.006% GDN, 10% glycerol, pH 8.0) and the complex was eluted with 20 ml of buffer A2 (50 mM Tris, 350 mM NaCl, 0.006% GDN, 10% glycerol, 2.5 mM desthiobiotin, pH 8.0) in 2-ml fractions. The fractions containing FtsQK were pooled, bound to an equilibrated 1-ml HisTrap column (Cytiva) and eluted using a step gradient from buffer B1 (50 mM Tris, 350 mM NaCl, 0.006% GDN, 10% Glycerol, 20 mM imidazole, pH 8.0) to buffer B2 (50 mM Tris, 350 mM NaCl, 0.006% GDN, 10% glycerol, 1 M imidazole, pH 8). The elution was concentrated to 50 µl using a 100-kDa cut-off centrifugal concentrator before further purification using a Superose 6 Increase 3.2/300 size-exclusion column in SEC buffer (50 mM Tris, 100 mM NaCl, 0.006% GDN, 10% glycerol, pH 8.0).

S. aureus PBP4

His-tagged *Sa*PBP4$^{21–383}$ was expressed as described previously[42] and purified as follows. Cells were lysed in buffer A (50 mM Tris, pH 7.5, 500 mM NaCl) containing 1 mM PMSF, DNase, RNase and protease inhibitor tablets using a cell disruptor at 25 kpsi. The lysate was centrifuged at 100,000*g* for 30 min. The supernatant was supplemented with 1% buffer B (buffer A + 1 M imidazole, pH 7.5) and cycled twice over a 5-ml HisTrap HP column (Cytiva). The column was washed with 150 ml 1% B, 550 ml 2% B and eluted in steps of 5, 30 and 50% B. Fractions containing *Sa*PBP4 were concentrated by centrifugal filtration (Vivaspin) and further purified over a Superdex 200 PG 16/60 size-exclusion column (Cytiva) in SEC buffer (20 mM MES, pH 6.0, 300 mM NaCl). Monomer peak fractions were combined and concentrated to 52 g l^{-1} by centrifugal filtration, then flash-frozen in aliquots before being stored at −80 °C.

Cryo-EM single-particle structure determination

Grid preparation for *Pa*FtsWIQBL. Grids were prepared with freshly purified protein from the peak fraction of the SEC elution at a final concentration of 1.2–1.3 g l^{-1}, diluting with SEC buffer if necessary. Then, 3 µl of sample were pipetted onto a glow-discharged (PELCO easiGlow, 25 mA, 45 s) 300 mesh copper 0.6/1 grid (Quantifoil) and blotted for 4 s at blot force 4, 100% humidity and 4 °C, before plunge-freezing in liquid ethane using a Vitrobot Mark IV (Thermo Fisher Scientific).

Grid preparation for *Ec*FtsWIQBL. Grids were prepared with freshly purified protein (*Ec*FtsWIQBL reconstituted in nanodiscs) from the peak fraction of the SEC elution at a final concentration of 0.5 g l^{-1} and diluted with SEC buffer if required. Then, 3 µl of sample were pipetted onto a freshly glow-discharged (30 mA, 60 s) 300 mesh UltraAu 0.6/1 grid (Quantifoil). After a 20-s wait time, the grids were blotted for 2.5 s at strength 5, 100% humidity and 10 °C, before plunge-freezing in liquid ethane using a Vitrobot Mark IV.

Data collection for *Pa*FtsWIQBL. Data from 5,531 micrographs were collected on a Titan Krios G3 (Thermo Fisher Scientific) equipped with a Gatan K3 camera and a Gatan Quantum energy filter (20 eV slit width). The EPU software was used to collect the micrographs with fringe-free imaging in counting mode at a nominal pixel size of 1.09 Å. The exposure time was 2.5 s at a dose of 21 e^-/px/s, defocus between −1.2 and −3 µm; 40 fractions per micrograph were collected.

Data collection for *Ec*FtsWIQBL. Data from 2,794 micrographs were collected on a Titan Krios G3 equipped with a Falcon 4 camera. The EPU software was used to collect the micrographs in counting mode at a nominal pixel size of 1.1 Å. The total dose was set to 39 $e^-/Å^2$ and defocus between −1.2 and −2.8 µm.

Data processing. Unless stated otherwise, all processing was done in RELION (v.4.0)[43]. Motion correction was performed using RELION's own implementation of the MotionCor2 algorithm[44] with 5 × 5 patches. CTFFind-4.1 (ref. 45) was used for CTF estimation. The initial reference was generated in CryoSPARC[46] from a different dataset of the same sample (not used for the final reconstruction). Particles were picked with Topaz[47] (7,276,623 particles in total, 1,398 per micrograph on average) and extracted 4× binned with a boxsize of 70 pixels (px) and a pixel size of 4.36 Å per px. The particles were split into seven subsets for initial three-dimensional (3D) classification into three classes. The best classes of each job were selected and refined. The refined particles were combined into two sets of particles and subjected to 3D classification without alignment. The best classes from each alignment were selected (1,997,326 and 2,922,553 particles in total), combined and subjected to 3D refinement. A mask (extended by 2 px and with added 2-px soft edge) was used to subtract the micelle density from the complex. The subtracted particles were subjected to 3D classification without alignment and two classes were selected (344,300 and 461,499 particles), re-extracted (2× binned with a boxsize of 140 px and a pixel size of 2.18 Å per px) and subjected to 3D refinement. 3D classification without alignment was run and the best class (160,615 particles) was selected. Particles were re-extracted (no binning, 280 px, 1.09 Å per px) and subjected to one round of polishing, as well 3D, CTF and 3D refinement. After subtraction of the micelle, the particles were subjected to a round of 3D refinement and 3D classification without alignment. From this 3D classification, the best class was selected (136,364 particles) and 3D-refined twice, the second time using a mask that excluded the POTRA domain of FtsQ. After post-processing with the calibrated pixel size (see below), the final reconstruction had an overall resolution of 3.7 Å as determined by Fourier shell correlation (cut-off of 0.143).

Model building. The pixel size was calibrated using Chimera[48]; a published crystal structure of *Pa*FtsI (Protein Data Bank (PDB) accession no. 3OCN) and subsequently adjusted to 1.05 Å per px during post-processing in RELION. This map was used to fit a model of *Pa*FtsWIQBL predicted with AF2 (refs. 24,49), manually adjusted using MAIN[50] and Coot[51] (v.0.9.8.3) and real-space refined using Phenix[52] (v.1.19.2-4158). Figures were prepared with ChimeraX-1.4 (ref. 53).

Lipid II extraction

Lipid II was extracted from *Enterococcus faecalis* (DSMZ 2570) as described previously[54]. Briefly, an overnight culture of *E. faecalis* was diluted 1:100 into 3 l of brain heart infusion (BHI) (Merck) and grown at 37 °C, 180 rpm to an OD_{600} of 0.7. Vancomycin (Sigma-Aldrich) and moenomycin (Santa Cruz Biotechnology) were added at 10 µg ml^{-1} and 5 µg ml^{-1}, respectively; after 20 min, cells were centrifuged in pre-cooled bottles at 4,500*g* for 20 min. Cell pellets were resuspended in BHI, centrifuged in Falcon tubes at 3,200*g* for 10 min, flash-frozen and stored at −20 °C overnight. Frozen cell pellets were thawed in a total of 30 ml PBS, divided equally into two 250-ml glass Erlenmeyer flasks; 17.5 ml chloroform and 35 ml methanol were added. After 2 h of vigorously stirring at room temperature, the mixture was spun in Teflon tubes for 10 min at 4,000*g* at 4 °C and the supernatant from each Erlenmeyer flask was combined with 30 ml chloroform and 22.5 ml PBS. The mixture was stirred vigorously for 2 h at room temperature, then spun for 10 min at 4,000*g* at 4 °C. The tubes were left at room temperature for 1 h until the supernatant was clear. The interface was then transferred with a glass Pasteur pipette to a 25-ml separatory funnel and left to settle overnight at 4 °C. The lower organic phase was discarded and the interface dried in a 25-ml round bottom flask on a rotary evaporator at 40 °C. The dried interface was resuspended in 7.5 ml pyridinium acetate:n-butanol (1:2) (PB) and 7.5 ml n-butanol-saturated water. Pyridinium acetate was prepared by adding 51.5 ml glacial acetic acid dropwise to 48.5 ml pyridine and filtered before use. The Lipid II extract was transferred to a 25-ml separatory funnel and the bottom phase was re-extracted with 5 ml PB. The top phase from the re-extraction was added to the top phase in the separatory funnel

and extracted three times with 5 ml n-butanol-saturated water. The top phase was dried using a rotary evaporator at 40 °C and resuspended in chloroform:methanol (1:1), partially dried under a stream of nitrogen gas and then transferred to a 250-µl non-stick glass vial (Agilent), in which it was dried completely. This was repeated four times to ensure efficient transfer before resuspending the Lipid II extract in 210 µl chloroform:methanol (1:1). The Lipid II extract was assessed by spotting 1–2 µl on an HPTLC silica gel 60F254 plate (Merck). The thin-layer chromatography plate was developed in a mixture of chloroform:methanol:water:ammonia (88:48:10:1) and Lipid II was visualized by heating the plate after soaking in phosphomolybdic acid as described previously[55].

Deprotection of Fluorenylmethoxycarbonyl-D-Lys-Biotin

D-Lys-Biotin was prepared according to a standard deprotection protocol[42]. Briefly, 15 mg Fluorenylmethoxycarbonyl-D-Lys(Biotin)-OH (Santa Cruz Biotechnology) was stirred in 3.1 ml of 20% piperidine/dimethylformamide and 466 µl toluene for 40 min at room temperature, then dried in a vacuum at 50 °C. The sample was resuspended in 5 ml water, stirred for 2 h at room temperature and then filtered through a 0.22-µm filter. The filtrate was pipetted into a tared tube, frozen on dry ice and then freeze-dried. The residue was dissolved in water to make a 10-mM stock, aliquoted and stored at −20 °C.

TG activity assay

Lipid II used to monitor glycosyltransferase activity of the protein complex was dried using a nitrogen stream and dissolved in an equal volume of dimethyl sulfoxide (DMSO). The reaction and detection of glycan strands was adopted from previously published protocols[3,23,42,56]. Briefly, *Pa*FtsWIQBL and *Ec*FtsWIQBL were mixed at a final protein concentration of 1 µM in 10 µl with 1 µl 10× reaction buffer (500 mM Tris, pH 7.5, 200 mM $MnCl_2$), 1 µl DMSO and 1 µl Lipid II and incubated for 30 min at 25 °C. Proteins were heat-inactivated for 2 min at 95 °C. Lipid II and glycan strands were labelled by incubating the reaction with 26 µM *Sa*PBP4 and 20 mM D-Lys-Biotin for 1 h at 25 °C. An equal volume of Laemmli SDS–PAGE buffer was added and the mixtures were heat-inactivated for 3 min at 95 °C. Glycan strands were separated from Lipid II on a 4–20% Criterion TGX polyacrylamide gel (Bio-Rad Laboratories), and run for 45 min at 200 V. After blotting onto a polyvinylidene fluoride membrane, the blot was incubated for 2 h in SuperBlock Blocking Buffer TBS (Thermo Fisher Scientific), followed by incubation with a 1:5,000 dilution of IRDye800CW Streptavidin (LI-COR Biosciences) in Tris-buffered saline at room temperature for 1 h. The blot was washed three times in PBS buffer and bands were visualized using an Odyssey CLx imaging system (LI-COR Biosciences).

Electron cryotomography of *E. coli* cells

A culture of *E. coli* strain B/r H266 expressing plasmid pRBJ212 (ref. 57) was grown in lysogeny broth medium at 37 °C, 180 rpm to an OD_{600} of 0.6. Cells were concentrated 10× by centrifugation and mixed with 10 nm protein A gold fiducials at a 1:10 ratio. Then, 4 µl of this mixture was applied to a 200-mesh copper 2 × 2 grid (Quantifoil), back-blotted and plunge-frozen in liquid ethane using a manual plunger. Cells were thinned by cryo-focused ion beam milling using a Scios dual beam FIB SEM (Thermo Fisher Scientific). Before milling, grids were sputtered with a protective layer of organic platinum using a gas injection system. Lamellae were milled in a stepwise fashion, gradually reducing the beam current as the lamellae were thinned, from 1 nA to 30 pA and at a nominal milling angle of 10°. Electron cryotomography was carried out on a Krios microscope equipped with a Gatan imaging filter and K2 camera. Tilt series were collected using the serialEM software[58], using a bidirectional tilt scheme from −10° (to flatten the lamella) with a 2° increment and a total dose of 112 $e^-/Å^2$, divided over 56 images, each with 10 frames. The pixel size was 3.7 Å and the defocus target was −5 µm. Frame and tilt series alignments were performed using IMOD[59]; 2× binned aligned tilt series were generated and used to generate a SIRT reconstruction using tomo3D[60], which were then low-pass-filtered to 20 Å.

Reporting summary

Further information on research design is available in the Nature Portfolio Reporting Summary linked to this article.

Data availability

The final cryo-EM map has been deposited in the Electron Microscopy Data Bank under accession no. EMD-16042. The final model has been deposited with the PDB under accession no. 8BH1. The PDB entries 6H9N, 3PBN, 5Z2W, 6BAS, 6PL5, 3OCN were used for structural superposition, analyses and pixel size calibration. Source data are provided with this paper.

References

1. Daley, D. O., Skoglund, U. & Söderström, B. FtsZ does not initiate membrane constriction at the onset of division. *Sci. Rep.* **6**, 33138 (2016).
2. Lutkenhaus, J., Pichoff, S. & Du, S. Bacterial cytokinesis: from Z ring to divisome. *Cytoskeleton* **69**, 778–790 (2012).
3. Taguchi, A. et al. FtsW is a peptidoglycan polymerase that is functional only in complex with its cognate penicillin-binding protein. *Nat. Microbiol.* **4**, 587–594 (2019).
4. Kumar, S., Mollo, A., Kahne, D. & Ruiz, N. The bacterial cell wall: from Lipid II flipping to polymerization. *Chem. Rev.* **122**, 8884–8910 (2022).
5. Egan, A. J., van't Veer, I., Breukink, E. & Vollmer, W. Activities and regulation of peptidoglycan synthases.*Philos. Trans. R Soc. Lond. B Biol. Sci.* **370**, 20150031 (2015).
6. Egan, A. J. F., Errington, J. & Vollmer, W. Regulation of peptidoglycan synthesis and remodelling. *Nat. Rev. Microbiol.* **18**, 446–460 (2020).
7. Marmont, L. S. & Bernhardt, T. G. A conserved subcomplex within the bacterial cytokinetic ring activates cell wall synthesis by the FtsW-FtsI synthase. *Proc. Natl Acad. Sci. USA* **117**, 23879–23885 (2020).
8. Liu, Y. & B, E. The membrane steps of bacterial cell wall synthesis as antibiotic targets. *Antibiotics* **5**, 28 (2016).
9. Lomize, M. A., Pogozheva, I. D., Joo, H., Mosberg, H. I. & Lomize, A. L. OPM database and PPM web server: resources for positioning of proteins in membranes. *Nucleic Acids Res.* **40**, D370–D376 (2012).
10. van den Ent, F. et al. Structural and mutational analysis of the cell division protein FtsQ. *Mol. Microbiol.* **68**, 110–123 (2008).
11. Kureisaite-Ciziene, D. et al. Structural analysis of the interaction between the bacterial cell division proteins FtsQ and FtsB.*mBio* **9**, e01346-18 (2018).
12. Choi, Y. et al. Structural insights into the FtsQ/FtsB/FtsL complex, a key component of the divisome. *Sci. Rep.* **8**, 18061 (2018).
13. Khadria, A. S. & Senes, A. The transmembrane domains of the bacterial cell division proteins FtsB and FtsL form a stable high-order oligomer. *Biochemistry* **52**, 7542–7550 (2013).
14. Condon, S. G. F. et al. The FtsLB subcomplex of the bacterial divisome is a tetramer with an uninterrupted FtsL helix linking the transmembrane and periplasmic regions. *J. Biol. Chem.* **293**, 1623–1641 (2018).
15. LaPointe, L. M. et al. Structural organization of FtsB, a transmembrane protein of the bacterial divisome. *Biochemistry* **52**, 2574–2585 (2013).
16. Robichon, C., Karimova, G., Beckwith, J. & Ladant, D. Role of leucine zipper motifs in association of the *Escherichia coli* cell division proteins FtsL and FtsB. *J. Bacteriol.* **193**, 4988–4992 (2011).
17. Buddelmeijer, N. & Beckwith, J. A complex of the *Escherichia coli* cell division proteins FtsL, FtsB and FtsQ forms independently of its localization to the septal region. *Mol. Microbiol.* **52**, 1315–1327 (2004).

18. Sjodt, M. et al. Structural coordination of polymerization and crosslinking by a SEDS–bPBP peptidoglycan synthase complex. *Nat. Microbiol* **5**, 813–820 (2020).
19. Park, K.-T., Du, S. & Lutkenhaus, J. Essential role for FtsL in activation of septal peptidoglycan synthesis. *mBio* **11**, e03012-20 (2020).
20. Han, S. et al. Structural basis for effectiveness of siderophore-conjugated monocarbams against clinically relevant strains of *Pseudomonas aeruginosa*. *Proc. Natl Acad. Sci. USA* **107**, 22002–22007 (2010).
21. Paulussen, F. M. et al. Covalent proteomimetic inhibitor of the bacterial FtsQB divisome complex. *J. Am. Chem. Soc.* **144**, 15303–15313 (2022).
22. Egan, A. J., Cleverley, R. M., Peters, K., Lewis, R. J. & Vollmer, W. Regulation of bacterial cell wall growth. *FEBS J.* **284**, 851–867 (2017).
23. Sjodt, M. et al. Structure of the peptidoglycan polymerase RodA resolved by evolutionary coupling analysis. *Nature* **556**, 118–121 (2018).
24. Jumper, J. et al. Highly accurate protein structure prediction with AlphaFold. *Nature* **596**, 583–589 (2021).
25. Shlosman, I. *et al*. Allosteric activation of cell wall synthesis during bacterial growth. Preprint at *bioRxiv* https://doi.org/10.1101/2022.11.07.515454 (2022).
26. Gerding, M. A. et al. Self-enhanced accumulation of FtsN at division sites and roles for other proteins with a SPOR domain (DamX, DedD, and RlpA) in *Escherichia coli* cell constriction. *J. Bacteriol.* **191**, 7383–7401 (2009).
27. Weiss, D. S. Last but not least: new insights into how FtsN triggers constriction during *Escherichia coli* cell division. *Mol. Microbiol.* **95**, 903–909 (2015).
28. Wissel, M. C. & Weiss, D. S. Genetic analysis of the cell division protein FtsI (PBP3): amino acid substitutions that impair septal localization of FtsI and recruitment of FtsN. *J. Bacteriol.* **186**, 490–502 (2004).
29. Chen, J. C. & Beckwith, J. FtsQ, FtsL and FtsI require FtsK, but not FtsN, for co-localization with FtsZ during *Escherichia coli* cell division. *Mol. Microbiol.* **42**, 395–413 (2001).
30. Addinall, S. G., Cao, C. & Lutkenhaus, J. FtsN, a late recruit to the septum in *Escherichia coli*. *Mol. Microbiol.* **25**, 303–309 (1997).
31. Liu, B., Persons, L., Lee, L. & de Boer, P. A. J. Roles for both FtsA and the FtsBLQ subcomplex in FtsN-stimulated cell constriction in *Escherichia coli*. *Mol. Microbiol.* **95**, 945–970 (2015).
32. Tsang, M.-J. & Bernhardt, T. G. A role for the FtsQLB complex in cytokinetic ring activation revealed by an *ftsL* allele that accelerates division. *Mol. Microbiol.* **95**, 925–944 (2015).
33. Ghigo, J. M. & Beckwith, J. Cell division in *Escherichia coli*: role of FtsL domains in septal localization, function, and oligomerization. *J. Bacteriol.* **182**, 116–129 (2000).
34. Li, Y. et al. Genetic analysis of the septal peptidoglycan synthase FtsWI complex supports a conserved activation mechanism for SEDS-bPBP complexes. *PLoS Genet.* **17**, e1009366 (2021).
35. Goehring, N. W., Gueiros-Filho, F. & Beckwith, J. Premature targeting of a cell division protein to midcell allows dissection of divisome assembly in *Escherichia coli*. *Genes Dev.* **19**, 127–137 (2005).
36. Hopf, T. A. et al. The EVcouplings Python framework for coevolutionary sequence analysis. *Bioinformatics* **35**, 1582–1584 (2019).
37. Weissmann, F. et al. biGBac enables rapid gene assembly for the expression of large multisubunit protein complexes. *Proc. Natl Acad. Sci. USA* **113**, E2564–E2569 (2016).
38. van den Berg van Saparoea, H. B. et al. Fine-mapping the contact sites of the *Escherichia coli* cell division proteins FtsB and FtsL on the FtsQ protein. *J. Biol. Chem.* **288**, 24340–24350 (2013).
39. Bieniossek, C., Richmond, T. J. & Berger, I. MultiBac: multigene baculovirus-based eukaryotic protein complex production. *Curr. Protoc. Protein Sci.* **Chapter 5**, Unit 5.20 (2008).
40. Laverty, D. et al. Cryo-EM structure of the human α1β3γ2 $GABA_A$ receptor in a lipid bilayer. *Nature* **565**, 516–520 (2019).
41. Ritchie, T. K. et al. Chapter 11—reconstitution of membrane proteins in phospholipid bilayer nanodiscs. *Methods Enzymol.* **464**, 211–231 (2009).
42. Qiao, Y. et al. Detection of lipid-linked peptidoglycan precursors by exploiting an unexpected transpeptidase reaction. *J. Am. Chem. Soc.* **136**, 14678–14681 (2014).
43. Scheres, S. H. W. A Bayesian view on cryo-EM structure determination. *J. Mol. Biol.* **415**, 406–418 (2012).
44. Zheng, S. Q. et al. MotionCor2: anisotropic correction of beam-induced motion for improved cryo-electron microscopy. *Nat. Methods* **14**, 331–332 (2017).
45. Rohou, A. & Grigorieff, N. CTFFIND4: fast and accurate defocus estimation from electron micrographs. *J. Struct. Biol.* **192**, 216–221 (2015).
46. Punjani, A., Rubinstein, J. L., Fleet, D. J. & Brubaker, M. A. cryoSPARC: algorithms for rapid unsupervised cryo-EM structure determination. *Nat. Methods* **14**, 290–296 (2017).
47. Bepler, T. et al. Positive-unlabeled convolutional neural networks for particle picking in cryo-electron micrographs. *Nat. Methods* **16**, 1153–1160 (2019).
48. Pettersen, E. F. et al. UCSF Chimera—a visualization system for exploratory research and analysis. *J. Comput. Chem.* **25**, 1605–1612 (2004).
49. Mirdita, M. et al. ColabFold: making protein folding accessible to all. *Nat. Methods* **19**, 679–682 (2022).
50. Turk, D. MAIN software for density averaging, model building, structure refinement and validation. *Acta Crystallogr. D Biol. Crystallogr.* **69**, 1342–1357 (2013).
51. Emsley, P., Lohkamp, B., Scott, W. G. & Cowtan, K. Features and development of Coot. *Acta Crystallogr. D Biol. Crystallogr.* **66**, 486–501 (2010).
52. Liebschner, D. et al. Macromolecular structure determination using X-rays, neutrons and electrons: recent developments in Phenix. *Acta Crystallogr. D Struct. Biol.* **75**, 861–877 (2019).
53. Pettersen, E. F. et al. UCSF ChimeraX: structure visualization for researchers, educators, and developers. *Protein Sci.* **30**, 70–82 (2021).
54. Welsh, M. A. et al. Identification of a functionally unique family of penicillin-binding proteins. *J. Am. Chem. Soc.* **139**, 17727–17730 (2017).
55. Schneider, T. et al. In vitro assembly of a complete, pentaglycine interpeptide bridge containing cell wall precursor (lipid II-Gly5) of *Staphylococcus aureus*. *Mol. Microbiol.* **53**, 675–685 (2004).
56. Barrett, D. et al. Analysis of glycan polymers produced by peptidoglycan glycosyltransferases. *J. Biol. Chem.* **282**, 31964–31971 (2007).
57. Salje, J. & Löwe, J. Bacterial actin: architecture of the ParMRC plasmid DNA partitioning complex. *EMBO J.* **27**, 2230–2238 (2008).
58. Mastronarde, D. N. Automated electron microscope tomography using robust prediction of specimen movements. *J. Struct. Biol.* **152**, 36–51 (2005).
59. Kremer, J. R., Mastronarde, D. N. & McIntosh, J. R. Computer visualization of three-dimensional image data using IMOD. *J. Struct. Biol.* **116**, 71–76 (1996).
60. Agulleiro, J. I. & Fernandez, J. J. Fast tomographic reconstruction on multicore computers. *Bioinformatics* **27**, 582–583 (2011).
61. Ashkenazy, H. et al. ConSurf 2016: an improved methodology to estimate and visualize evolutionary conservation in macromolecules. *Nucleic Acids Res.* **44**, W344–W350 (2016).

Acknowledgements
We thank all members of the MRC LMB electron microscopy facility for excellent electron microscopy support and T. Darling and J. Grimmett for computing support. We thank D. Ritson and M. Su for their help and advice during the Lipid II preparation and H. Kramer (1979–2022) for the liquid chromatography–mass spectrometry and matrix-assisted laser desorption/ionization coupled to time-of-flight mass spectrometry of the Lipid II samples (all MRC LMB). N-terminal His-tagged *Sa*PBP4 (amino acids 21–383) was a gift of the Walker laboratory (Harvard). We thank S. Nayak (MRC LMB VisLabs) for her help with designing the figures. We thank T. Bharat and S. Tetter for their feedback on the manuscript. This work was supported by the Volkswagen Stiftung 'Life?' programme (to J.L.) and by the MRC as part of United Kingdom Research and Innovation. MRC file reference no. U105184326 (to J.L.). For the purpose of open access, the MRC Laboratory of Molecular Biology has applied a CC BY public copyright licence to any author-accepted manuscript version arising.

Author contributions
L.K., F.v.d.E. and M.J. purified the *Pa*FtsQBLWI complex. L.K. collected and processed the cryo-EM data of the *Pa*FtsQBLWI complex. F.v.d.E. and M.J. purified the *Ec*FtsQBLWI complex. M.J. collected and processed the cryo-EM data of the *Ec*FtsQBLWI complex. F.v.d.E. purified Lipid II and performed the FtsWIQBL activity assays. N.L.J. cloned and purified the FtsQ–FtsK complex. V.L.H. prepared, measured and processed the tomogram. J.L. provided the concept and L.K., M.J. and J.L. prepared the manuscript. All authors contributed to the Methods section and to editing the manuscript.

Competing interests
The authors declare no competing interests.

Additional information
Extended data is available for this paper at https://doi.org/10.1038/s41564-023-01368-0.

Supplementary information The online version contains supplementary material available at https://doi.org/10.1038/s41564-023-01368-0.

Correspondence and requests for materials should be addressed to Jan Löwe.

Peer review information *Nature Microbiology* thanks Oscar LLorca and the other, anonymous, reviewer(s) for their contribution to the peer review of this work.

Reprints and permissions information is available at www.nature.com/reprints.

Publisher's note Springer Nature remains neutral with regard to jurisdictional claims in published maps and institutional affiliations.

Springer Nature or its licensor (e.g. a society or other partner) holds exclusive rights to this article under a publishing agreement with the author(s) or other rightsholder(s); author self-archiving of the accepted manuscript version of this article is solely governed by the terms of such publishing agreement and applicable law.

© The Author(s), under exclusive licence to Springer Nature Limited 2023

https://doi.org/10.1038/s41564-023-01368-0

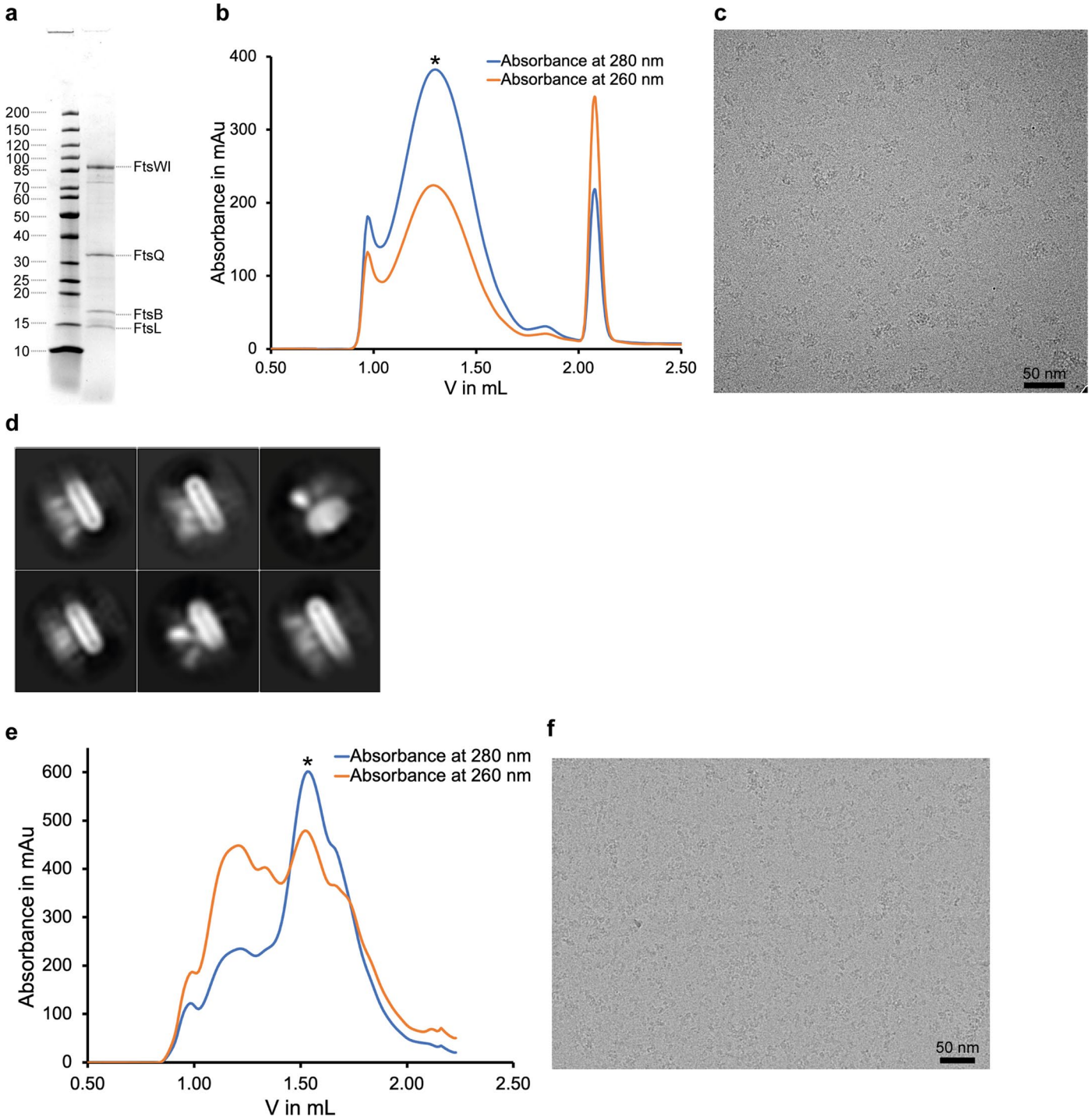

Extended Data Fig. 1 | Protein purification and grid preparation of FtsWIQBL from *E. coli* (*Ec*) and *P. aeruginosa* (*Pa*). a) SDS-PAGE gel of the co-expressed and purified *Ec*FtsWIQBL divisome core complex after size-exclusion chromatography in GDN. FtsW and FtsI are joined by a short linker in this construct. **b)** Size-exclusion chromatogram of *Ec*FtsWIQBL reconstituted in nanodiscs. The measured absorbances at 260 nm and 280 nm are shown in orange and blue, respectively. The peak fraction of the size exclusion run, indicated with an asterisk, was used for grid preparation. **c)** Representative micrograph of *Ec*FtsWIQBL in nanodiscs. **d)** Representative 2D Classes of *Ec*FtsWIQBL in nanodiscs. **e)** Size-exclusion chromatogram of *Pa*FtsWIQBL. The measured absorbances at 260 nm and 280 nm are shown in orange and blue, respectively. The peak fraction of the size exclusion run, indicated with an asterisk, was used for grid preparation. **f)** Representative micrograph of *Pa*FtsWIQBL used for the final reconstruction.

https://doi.org/10.1038/s41564-023-01368-0

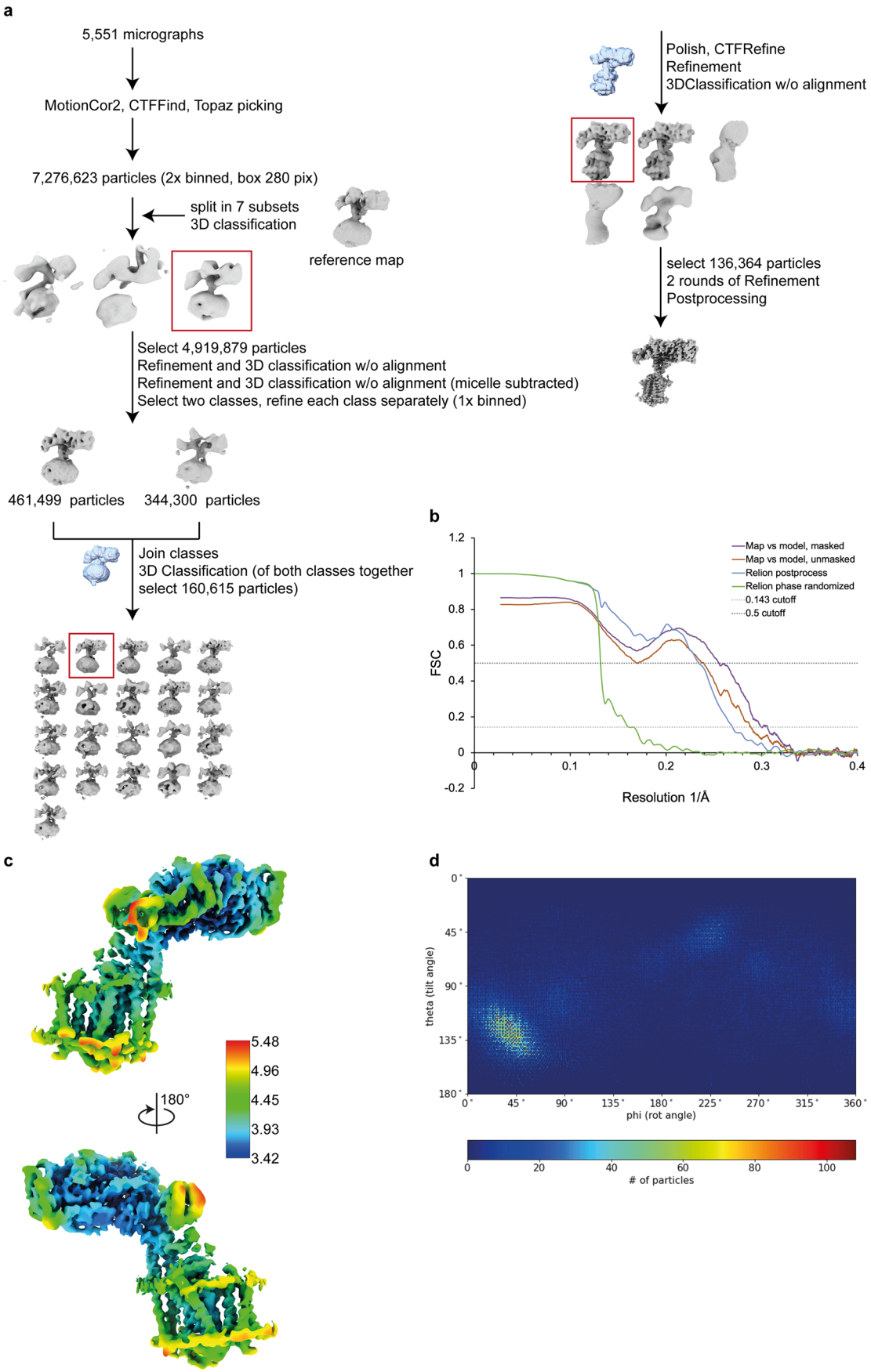

Extended Data Fig. 2 | Details of the *Pa*FtsWIQBL cryo-EM processing. **a)** Cryo-EM image processing scheme for *Pa*FtsWIQBL. **b)** Fourier Shell Correlation (FSC) curves for the *Pa*FtsWIQBL cryo-EM maps and structures. **c)** The local resolution of the final structure of *Pa*FtsWIQBL was calculated with RELION's own implementation and depicted in ChimeraX[53]. **d)** The angular distribution of the particles making up the final structure of *Pa*FtsWIQBL.

https://doi.org/10.1038/s41564-023-01368-0

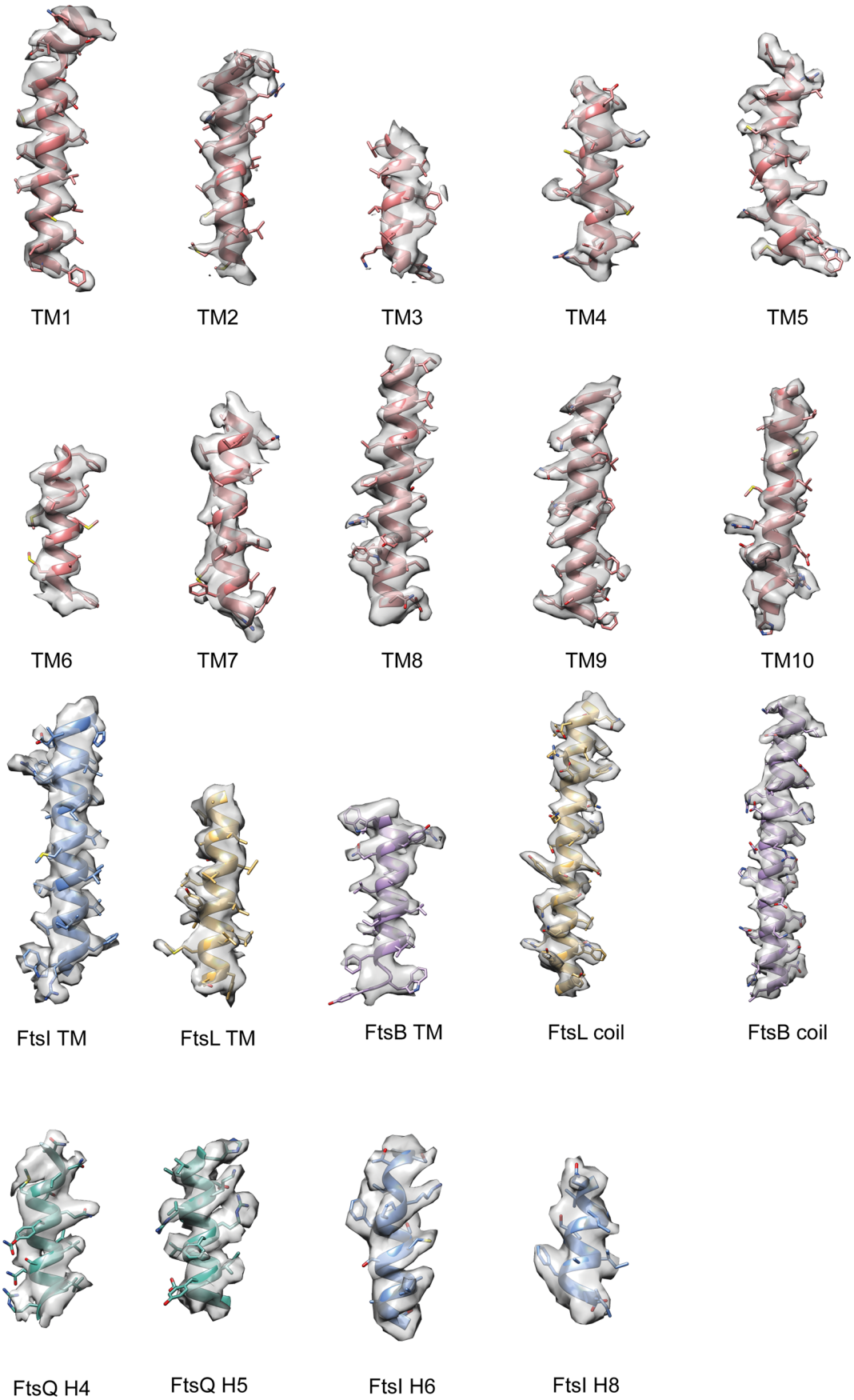

Extended Data Fig. 3 | Details of the cryo-EM density around helices of *Pa*FtsWIQBL. All TM helices visible in the structure are shown, as well as the FtsL$^{\alpha 1}$ and FtsB $^{\alpha 2}$ coils, two helices from FtsQ$^{\beta}$ and two helices from the FtsI^{TP} domain.

https://doi.org/10.1038/s41564-023-01368-0

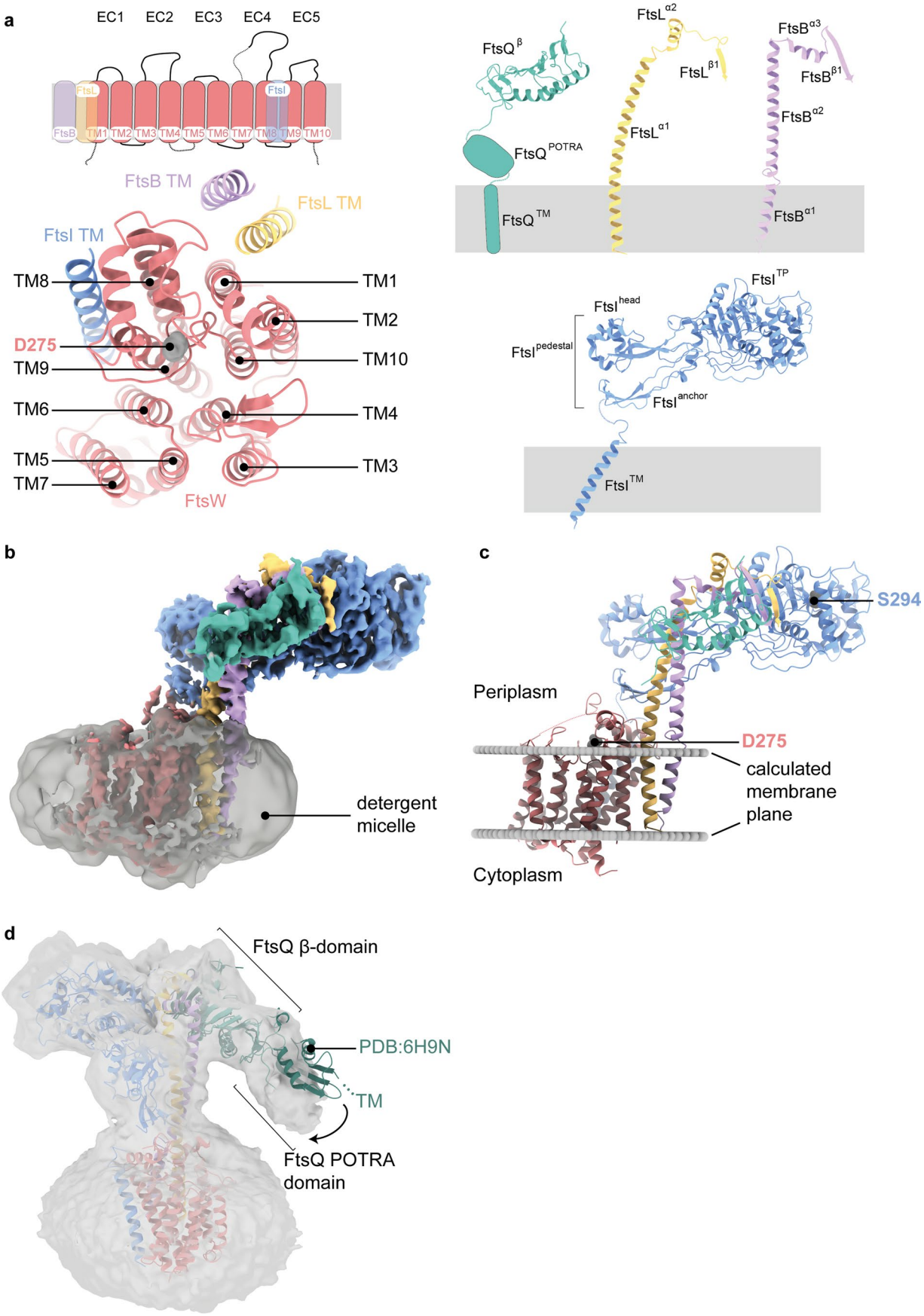

Extended Data Fig. 4 | See next page for caption.

https://doi.org/10.1038/s41564-023-01368-0

Extended Data Fig. 4 | Architecture of the *Pa*FtsWIQBL complex. a) Upper left panel: schematic of the transmembrane helices of FtsW, FtsI, FtsL and FtsB. Two extracellular loops of FtsW that could not be build due to missing density and the N- and C-terminal tails of FtsW are indicated by doted lines. Lower left panel: top view of the transmembrane domain, with FtsW transmembrane helices consecutively numbered based on the sequence (identical to numbering of helices in a previous RodA structure[23]). FtsW's putative active site residue D275 is indicated. Right panel: Labelling of the different domains in FtsQ, FtsL, FtsB and FtsI that was used throughout the paper. **b)** Cryo-EM density showing *Pa*FtsWIQBL within the Lauryl Maltose Neopentyl Glycol (LMNG) detergent micelle, which was subtracted during the later processing stages. **c)** Prediction of the position and orientation of the divisome core complex transmembrane segments in the lipid bilayer using the Orientations of Proteins in Membranes webserver[9]. The membrane plane is indicated with two grey discs and the active sites of FtsW and FtsI are labelled. **d)** A low-resolution structure obtained after fewer 3D classifications shows additional density for $FtsQ^{POTRA}$ at low contour levels and indicates that the transmembrane segment of FtsQ is most likely not part of the micelle that contains the other TM segments. Alignment of a previous FtsB:FtsQ crystal structure (PDB: 6H9N) on $FtsQ^{\beta}$ shows that $FtsQ^{\beta}$ and $FtsQ^{POTRA}$ adopt different conformations relative to each other.

https://doi.org/10.1038/s41564-023-01368-0

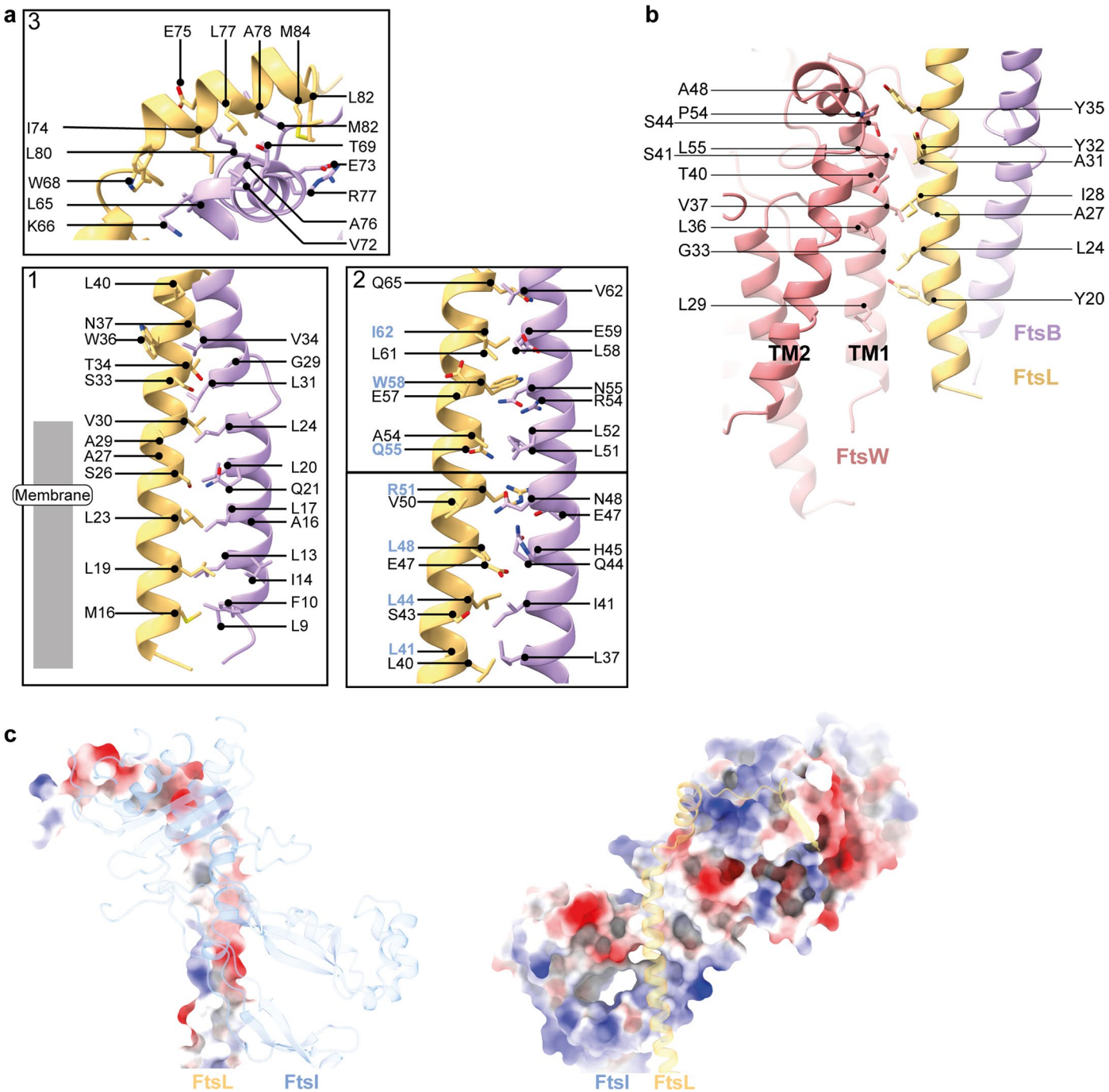

Extended Data Fig. 5 | Detailed analysis of the interactions between FtsB and FtsL, FtsW and FtsL and FtsI and FtsL. a) Interaction sites between FtsB and FtsL, as also indicated in Fig. 2a. Residues of FtsL that also interact with FtsI are highlighted in blue. **b)** Analysis of the interaction sites between FtsL and FtsW in their transmembrane region. The coiled coil conformation of FtsL means that the interaction surface is not as extended as it would be if it were straighter and not in a coiled coil. **c)** Electrostatic analysis of the interactions between FtsI and FtsL shows that the interaction site in the coiled coil area is mainly hydrophobic/neutral.

https://doi.org/10.1038/s41564-023-01368-0

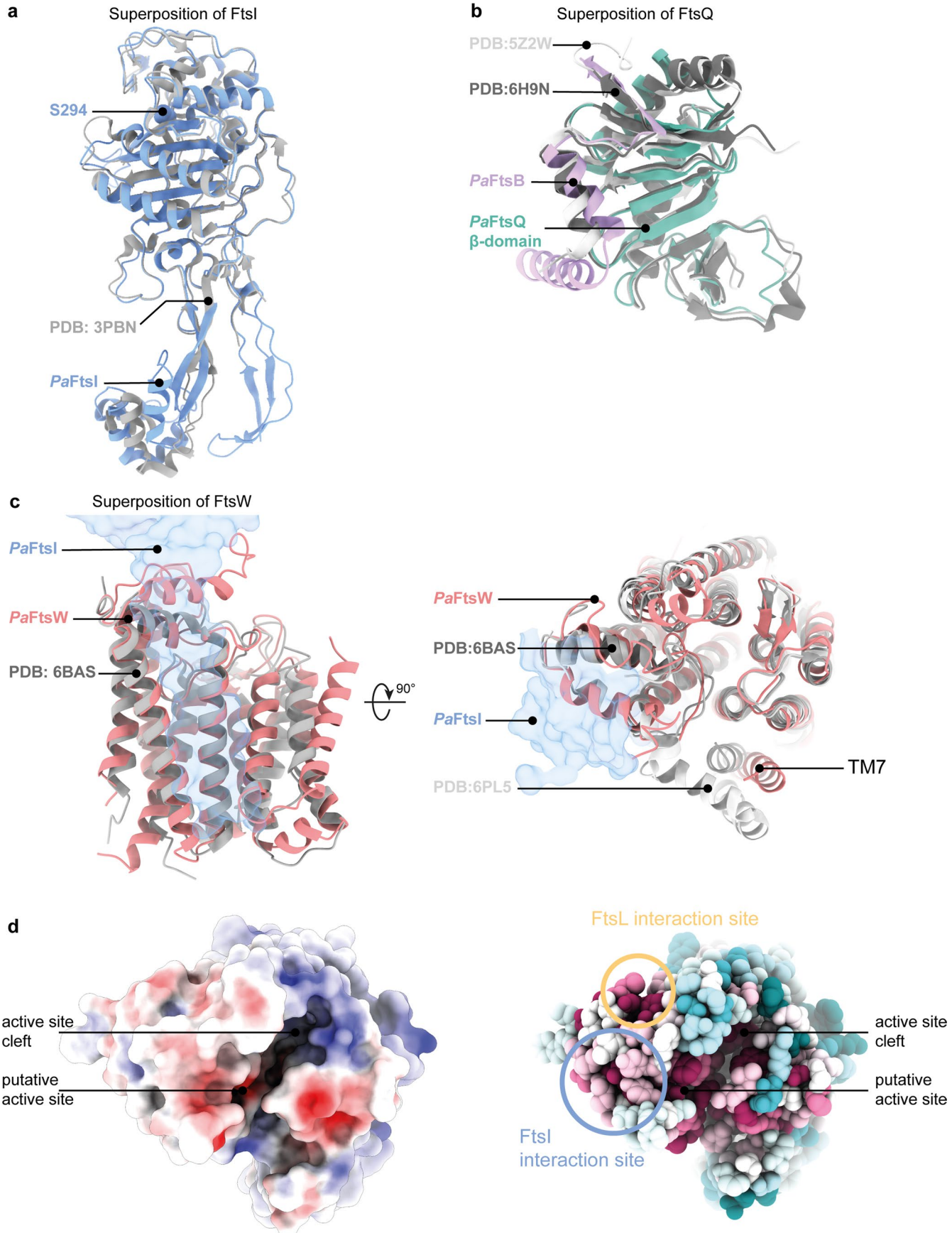

Extended Data Fig. 6 | See next page for caption.

https://doi.org/10.1038/s41564-023-01368-0

Extended Data Fig. 6 | Comparison of *Pa*FtsWIQBL cryo-EM structure with previous crystal structures of FtsI, FtsQ and RodA. a) Superposition of FtsI determined by X-ray crystallography (PDB: 3PBN, grey) with the FtsI part of *Pa*FtsWIQBL cryo-EM structure. The TP active site residue S294 is indicated (RMSD of 0.708 Å across 372 pruned atom pairs). **b)** Superposition of FtsQB determined by X-ray crystallography (PDB: 6H9N in dark grey, PDB: 5Z2W in light grey) with the same area in the cryo-EM structure determined here (For alignment of FtsQ: RMSD (FtsQ-6H9N) of 1.186 Å across 86 pruned atom pairs, RMSD (FtsQ-5Z2W) of 1.118 Å across 95 pruned atom pairs). **c)** Superposition of RodA determined by X-ray crystallography (PDB: 6BAS in dark grey (left and right), PDB: 6PL5 in light gray (right)) and FtsW in the cryo-EM structure. The position of FtsI is indicated as a transparent blue outline. Apart from transmembrane helix 7, the structures align very well (RMSD (FtsW-6PL5) of 1.188 Å across 202 pruned atom pairs; RMSD (FtsW-6BAS) of 1.126 Å across 206 pruned atom pairs). **d)** Electrostatic surface representation of *Pa*FtsW viewed from the periplasmic side. A deep cleft is visible that contains the putative active site residue D275. The same representation showing sequence conservation of FtsW mapped onto the surface representation shows that this cleft is highly conserved. Additionally, interaction sites with FtsI and FtsL are indicated; these also show above average levels of sequence conservation.

https://doi.org/10.1038/s41564-023-01368-0

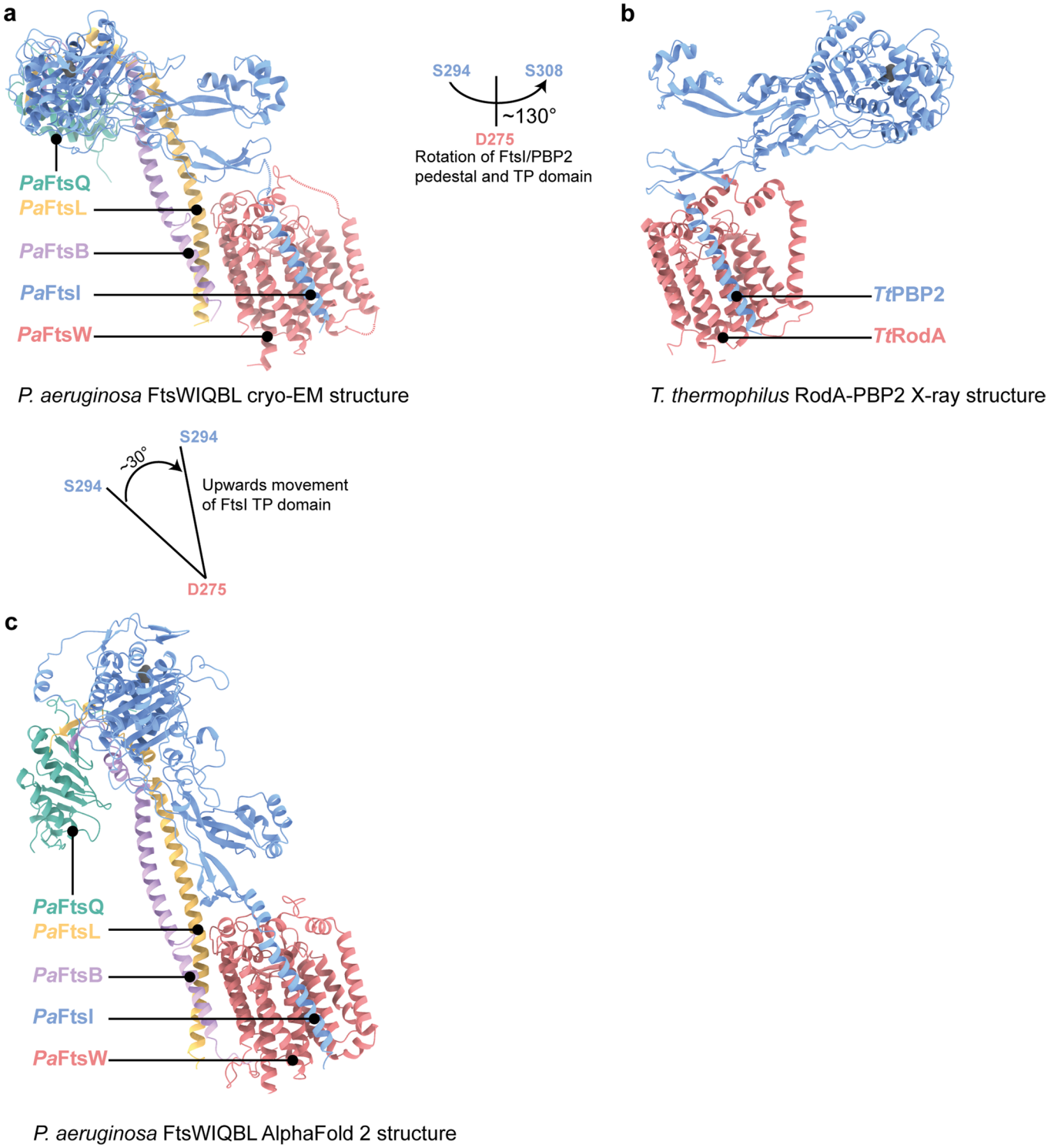

Extended Data Fig. 7 | Comparison of the *Pa*FtsWIQBL cryo-EM structure with a RodA-PBP2 crystal structure and AlphaFold 2 structure prediction. Comparison of the cryo-EM structure *Pa*FtsWIQBL **(a)**, the *Thermus thermophilus* RodA-PBP2 crystal structure (PDB: 6PL5, **b)** and the AlphaFold 2 prediction of *Pa*FtsWIQBL **(c)**. All three structures were aligned on FtsW/RodA. The $FtsQ^{POTRA}$ and $FtsQ^{TM}$ of the AlphaFold2 model were removed for clarity. The FtsI/PBP2 periplasmic domains show a large 130° lateral rotation between the *P. aeruginosa* FtsWI and *T. thermophilus* RodA-PBP2 models (a-b). The rotation was measured around an axis perpendicular to the membrane plane and intersecting the FtsW active site. The distance between both active sites in FtsI (S294) and PBP2 (S308) is 125 Å. A 30° vertical rotation of the periplasmic FtsI domains is visible between the cryo-EM and AlphaFold2 models of *Pa*FtsWIQBL (a-c). The angle was measured between the FtsW active site (D275) and the FtsI active sites (S294). The distance between the FtsI active sites in the cryo-EM and AlphaFold2 models is 46 Å.

https://doi.org/10.1038/s41564-023-01368-0

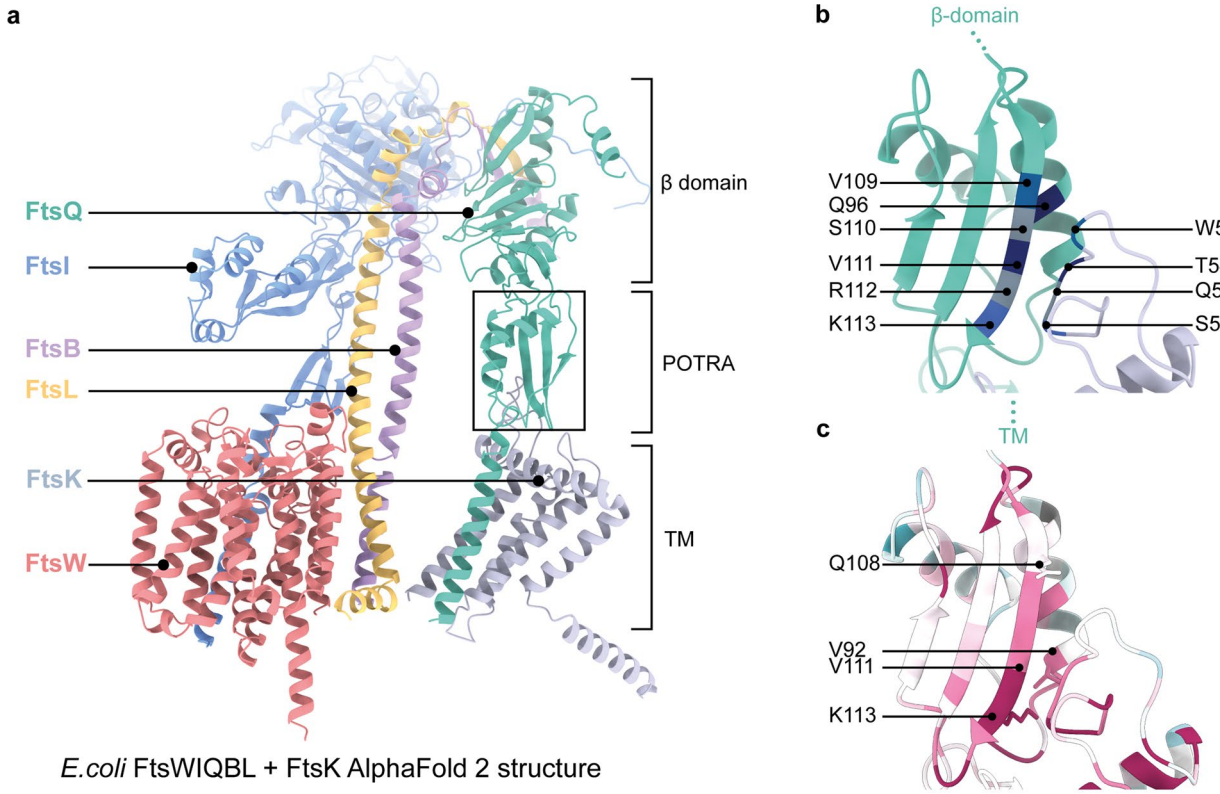

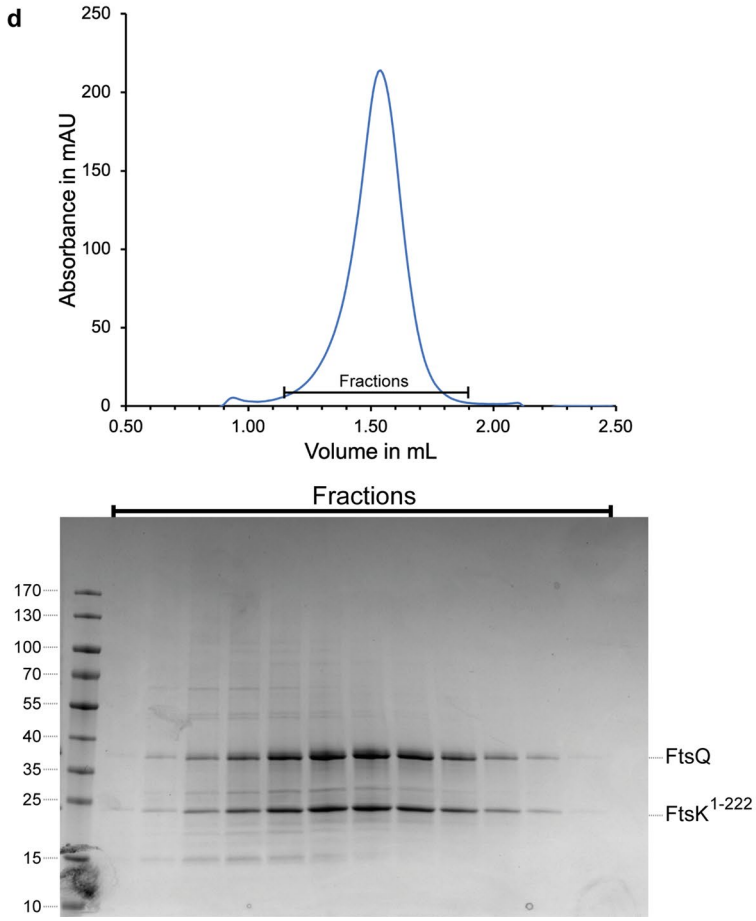

Extended Data Fig. 8 | See next page for caption.

https://doi.org/10.1038/s41564-023-01368-0

Extended Data Fig. 8 | Interactions of FtsQ with FtsK. a) AlphaFold2 model of *E. coli* FtsWIQBL + FtsK N-terminal domain (residues 1-222; $FtsK^{1-222}$, grey), showing a predicted interaction between $FtsQ^{POTRA}$ and a periplasmic loop from FtsK ($FtsK^{W51\text{-}H57}$). **b)** Co-evolutionary coupling analysis calculated with EVcouplings[36] finds six out of the ten residue pairs located between $FtsQ^{POTRA}$ and $FtsK^{W51\text{-}H57}$ in the AF2 model in a): $FtsQ^{V109}$ – $FtsK^{W56}$ (blue), $FtsQ^{Q96}$ – $FtsK^{T54}$ (dark blue), $FtsQ^{S110}$ – $FtsK^{Q53}$ (gray), $FtsQ^{V111}$ – $FtsK^{T54}$ (dark blue), $FtsQ^{R112}$ – $FtsK^{Q53}$ (grey), and $FtsQ^{K113}$-$FtsK^{S52}$ (blue). **c)** Sequence conservation analysis (calculated using ConSurf webserver[61]) of the same area shows that the β-strands of FtsQ and $FtsK^{W51\text{-}H57}$ that are predicted to interact are highly conserved. Amino acid residues that abolish FtsQ localisation (which is dependent on FtsK septum localisation in cells) when mutated are shown as sticks and are labelled[10]. **d)** Size-exclusion trace and SDS-PAGE gel of the co-expression and purification of *E. coli* FtsQ and $FtsK^{1-222}$ shows clear co-migration of the proteins.

nature portfolio

Corresponding author(s): Jan Löwe

Last updated by author(s): 21.03.2023

Reporting Summary

Nature Portfolio wishes to improve the reproducibility of the work that we publish. This form provides structure for consistency and transparency in reporting. For further information on Nature Portfolio policies, see our Editorial Policies and the Editorial Policy Checklist.

Statistics

For all statistical analyses, confirm that the following items are present in the figure legend, table legend, main text, or Methods section.

n/a	Confirmed	
☐	☒	The exact sample size (*n*) for each experimental group/condition, given as a discrete number and unit of measurement
☐	☒	A statement on whether measurements were taken from distinct samples or whether the same sample was measured repeatedly
☒	☐	The statistical test(s) used AND whether they are one- or two-sided *Only common tests should be described solely by name; describe more complex techniques in the Methods section.*
☒	☐	A description of all covariates tested
☒	☐	A description of any assumptions or corrections, such as tests of normality and adjustment for multiple comparisons
☒	☐	A full description of the statistical parameters including central tendency (e.g. means) or other basic estimates (e.g. regression coefficient) AND variation (e.g. standard deviation) or associated estimates of uncertainty (e.g. confidence intervals)
☒	☐	For null hypothesis testing, the test statistic (e.g. *F*, *t*, *r*) with confidence intervals, effect sizes, degrees of freedom and *P* value noted *Give P values as exact values whenever suitable.*
☒	☐	For Bayesian analysis, information on the choice of priors and Markov chain Monte Carlo settings
☒	☐	For hierarchical and complex designs, identification of the appropriate level for tests and full reporting of outcomes
☒	☐	Estimates of effect sizes (e.g. Cohen's *d*, Pearson's *r*), indicating how they were calculated

Our web collection on statistics for biologists contains articles on many of the points above.

Software and code

Policy information about availability of computer code

Data collection	Cryo-EM SPA data was collected with EPU (Version 2.14), Cryo-EM Tomography data was collected with SerialEM (Version 3.5)
Data analysis	CTFFind (Version 4.1) RELION (Version 4.0.0) MotionCor2 UCSF Chimera (Version 1.14.0) COOT (Version 0.9.8.3) MAIN (Version 2017) Phenix (Version 1.19.2-4158) UCSF ChimeraX (Version 1.4.0) CryoSPARC (Version v2.15.0) AlphaFold multimer (Version 2.2.0) Imod (Version 4.9) tomo3D (Version 2.0) Orientations of Proteins in Membranes webserver (PPM 2.0) ConSurf webserver EVcouplings webserver (v.1)

For manuscripts utilizing custom algorithms or software that are central to the research but not yet described in published literature, software must be made available to editors and reviewers. We strongly encourage code deposition in a community repository (e.g. GitHub). See the Nature Portfolio guidelines for submitting code & software for further information.

Data

Policy information about availability of data

All manuscripts must include a data availability statement. This statement should provide the following information, where applicable:

- Accession codes, unique identifiers, or web links for publicly available datasets
- A description of any restrictions on data availability
- For clinical datasets or third party data, please ensure that the statement adheres to our policy

The final cryo EM map has been deposited in the Electron Microscopy Data Bank (EMDB) with the accession code EMD-16042. The final model has been deposited with the Protein Data Bank (PDB) with the accession code 8BH1.
PDB entries 6H9N, 3PBN, 5Z2W, 6BAS, 6PL5, 3OCN were used for structural superposition, analyses and pixel size calibration. Source data are provided with this paper.
Uniprot accession codes for the purified complexes:
PaFtsWIQBL (Uniprot: Q9HW00 (FtsW), G3XD46 (FtsI), G3XDA7 (FtsQ), Q9HVZ6 (FtsL), Q9HXZ6 (FtsB))
EcFtsWIQBL (Uniprot: P0ABG4 (FtsW), P0AD68 (FtsI), P06136 (FtsQ), P0AEN4 (FtsL), P0A6S5 (FtsB))
EcFtsQK (Uniprot: P0613 (FtsQ), P46889 (FtsK))

Human research participants

Policy information about studies involving human research participants and Sex and Gender in Research.

Reporting on sex and gender	N/A
Population characteristics	N/A
Recruitment	N/A
Ethics oversight	N/A

Note that full information on the approval of the study protocol must also be provided in the manuscript.

Field-specific reporting

Please select the one below that is the best fit for your research. If you are not sure, read the appropriate sections before making your selection.

☒ Life sciences ☐ Behavioural & social sciences ☐ Ecological, evolutionary & environmental sciences

For a reference copy of the document with all sections, see nature.com/documents/nr-reporting-summary-flat.pdf

Life sciences study design

All studies must disclose on these points even when the disclosure is negative.

Sample size	Sample sizes were not predetermined and all available data was processed. For cryo-EM two datasets with 5531 micrographs (P. aeruginosa) and 2794 micrographs (E.coli) were collected and processed. Data of the PaFtsWIQBL sample was processed to a resolution of 3.7A which was sufficient for interpretation of the experimental data and to build an atomic model. For EcFtsWIQBL the sample did not reach high resolution which was not due to the sample size but the behaviour of the sample.
Data exclusions	Cryo-EM particle sorting and exclusion. For PaFtsWIQBL, 3D classification was used to sort the particles. Classes with low resolution were excluded. For EcFtsWIQBL 2D classification was used to sort particles into classes. Classes that contained contaminations were excluded. This followed standard cryo-EM processing procedure. Details for the processing are given in the manuscript.
Replication	PaFtsWIQBL: measurement of three datasets (different microscopes and number of micrographs) from different grids and two protein purifications that could be resolved to different resolutions and always showed the same conformation, all attempts of replication were successful resulting in the purification of the PaFtsWIQBL complex and data sets that at least could be processed to obtain well ordered 2D Classes EcFtsWIQBL: Thirteen protein purification preps in different detergents and nanodiscs and collected 14 datasets, every replication was successful Activity assay: EcFtsWIQBL 18 repeats from different fractions and different preps with and without nanodiscs were all positive. PaWIQBL 13 repeats in detergent from different fractions and different preps and a test in nanodiscs were all positive. PaW(D275A)IQBL was repeated 4 times and was negative. Lipid II purification: 12 preps with similar yields. EcFtsQK: The purification was repeated three times and all replications were successful. Tomography: The depicted tomogram was one representative example from tens of tomograms collected, every replication was successful

Randomization	No randomisation was performed. N/A for in vitro reconstitution with purified proteins
Blinding	No blinding was performed. N/A for this study since no experimental groups with participants like humans or animals were involved in the study

Behavioural & social sciences study design

All studies must disclose on these points even when the disclosure is negative.

Study description	*Briefly describe the study type including whether data are quantitative, qualitative, or mixed-methods (e.g. qualitative cross-sectional, quantitative experimental, mixed-methods case study).*
Research sample	*State the research sample (e.g. Harvard university undergraduates, villagers in rural India) and provide relevant demographic information (e.g. age, sex) and indicate whether the sample is representative. Provide a rationale for the study sample chosen. For studies involving existing datasets, please describe the dataset and source.*
Sampling strategy	*Describe the sampling procedure (e.g. random, snowball, stratified, convenience). Describe the statistical methods that were used to predetermine sample size OR if no sample-size calculation was performed, describe how sample sizes were chosen and provide a rationale for why these sample sizes are sufficient. For qualitative data, please indicate whether data saturation was considered, and what criteria were used to decide that no further sampling was needed.*
Data collection	*Provide details about the data collection procedure, including the instruments or devices used to record the data (e.g. pen and paper, computer, eye tracker, video or audio equipment) whether anyone was present besides the participant(s) and the researcher, and whether the researcher was blind to experimental condition and/or the study hypothesis during data collection.*
Timing	*Indicate the start and stop dates of data collection. If there is a gap between collection periods, state the dates for each sample cohort.*
Data exclusions	*If no data were excluded from the analyses, state so OR if data were excluded, provide the exact number of exclusions and the rationale behind them, indicating whether exclusion criteria were pre-established.*
Non-participation	*State how many participants dropped out/declined participation and the reason(s) given OR provide response rate OR state that no participants dropped out/declined participation.*
Randomization	*If participants were not allocated into experimental groups, state so OR describe how participants were allocated to groups, and if allocation was not random, describe how covariates were controlled.*

Ecological, evolutionary & environmental sciences study design

All studies must disclose on these points even when the disclosure is negative.

Study description	*Briefly describe the study. For quantitative data include treatment factors and interactions, design structure (e.g. factorial, nested, hierarchical), nature and number of experimental units and replicates.*
Research sample	*Describe the research sample (e.g. a group of tagged Passer domesticus, all Stenocereus thurberi within Organ Pipe Cactus National Monument), and provide a rationale for the sample choice. When relevant, describe the organism taxa, source, sex, age range and any manipulations. State what population the sample is meant to represent when applicable. For studies involving existing datasets, describe the data and its source.*
Sampling strategy	*Note the sampling procedure. Describe the statistical methods that were used to predetermine sample size OR if no sample-size calculation was performed, describe how sample sizes were chosen and provide a rationale for why these sample sizes are sufficient.*
Data collection	*Describe the data collection procedure, including who recorded the data and how.*
Timing and spatial scale	*Indicate the start and stop dates of data collection, noting the frequency and periodicity of sampling and providing a rationale for these choices. If there is a gap between collection periods, state the dates for each sample cohort. Specify the spatial scale from which the data are taken*
Data exclusions	*If no data were excluded from the analyses, state so OR if data were excluded, describe the exclusions and the rationale behind them, indicating whether exclusion criteria were pre-established.*
Reproducibility	*Describe the measures taken to verify the reproducibility of experimental findings. For each experiment, note whether any attempts to repeat the experiment failed OR state that all attempts to repeat the experiment were successful.*
Randomization	*Describe how samples/organisms/participants were allocated into groups. If allocation was not random, describe how covariates were controlled. If this is not relevant to your study, explain why.*

Blinding

Describe the extent of blinding used during data acquisition and analysis. If blinding was not possible, describe why OR explain why blinding was not relevant to your study.

Did the study involve field work? ☐ Yes ☐ No

Field work, collection and transport

Field conditions

Describe the study conditions for field work, providing relevant parameters (e.g. temperature, rainfall).

Location

State the location of the sampling or experiment, providing relevant parameters (e.g. latitude and longitude, elevation, water depth).

Access & import/export

Describe the efforts you have made to access habitats and to collect and import/export your samples in a responsible manner and in compliance with local, national and international laws, noting any permits that were obtained (give the name of the issuing authority, the date of issue, and any identifying information).

Disturbance

Describe any disturbance caused by the study and how it was minimized.

Reporting for specific materials, systems and methods

We require information from authors about some types of materials, experimental systems and methods used in many studies. Here, indicate whether each material, system or method listed is relevant to your study. If you are not sure if a list item applies to your research, read the appropriate section before selecting a response.

Materials & experimental systems

n/a	Involved in the study
☒	☐ Antibodies
☐	☒ Eukaryotic cell lines
☒	☐ Palaeontology and archaeology
☒	☐ Animals and other organisms
☒	☐ Clinical data
☒	☐ Dual use research of concern

Methods

n/a	Involved in the study
☒	☐ ChIP-seq
☒	☐ Flow cytometry
☒	☐ MRI-based neuroimaging

Antibodies

Antibodies used

Describe all antibodies used in the study; as applicable, provide supplier name, catalog number, clone name, and lot number.

Validation

Describe the validation of each primary antibody for the species and application, noting any validation statements on the manufacturer's website, relevant citations, antibody profiles in online databases, or data provided in the manuscript.

Eukaryotic cell lines

Policy information about cell lines and Sex and Gender in Research

Cell line source(s)

Sf9 cells, Oxford Expression Technologies Ltd, Cat No. 600100.

Authentication

None of the cell lines used were authenticated.

Mycoplasma contamination

For each batch of SF9, the cells were tested negative for Mycoplasma before use.

Commonly misidentified lines
(See ICLAC register)

No commonly misidentified cell lines were used in this study

Palaeontology and Archaeology

Specimen provenance

Provide provenance information for specimens and describe permits that were obtained for the work (including the name of the issuing authority, the date of issue, and any identifying information). Permits should encompass collection and, where applicable, export.

Specimen deposition

Indicate where the specimens have been deposited to permit free access by other researchers.

Dating methods

If new dates are provided, describe how they were obtained (e.g. collection, storage, sample pretreatment and measurement), where they were obtained (i.e. lab name), the calibration program and the protocol for quality assurance OR state that no new dates are provided.

☐ Tick this box to confirm that the raw and calibrated dates are available in the paper or in Supplementary Information.

Ethics oversight

Identify the organization(s) that approved or provided guidance on the study protocol, OR state that no ethical approval or guidance was required and explain why not.

Note that full information on the approval of the study protocol must also be provided in the manuscript.

Animals and other research organisms

Policy information about studies involving animals; ARRIVE guidelines recommended for reporting animal research, and Sex and Gender in Research

Laboratory animals

For laboratory animals, report species, strain and age OR state that the study did not involve laboratory animals.

Wild animals

Provide details on animals observed in or captured in the field; report species and age where possible. Describe how animals were caught and transported and what happened to captive animals after the study (if killed, explain why and describe method; if released, say where and when) OR state that the study did not involve wild animals.

Reporting on sex

Indicate if findings apply to only one sex; describe whether sex was considered in study design, methods used for assigning sex. Provide data disaggregated for sex where this information has been collected in the source data as appropriate; provide overall numbers in this Reporting Summary. Please state if this information has not been collected. Report sex-based analyses where performed, justify reasons for lack of sex-based analysis.

Field-collected samples

For laboratory work with field-collected samples, describe all relevant parameters such as housing, maintenance, temperature, photoperiod and end-of-experiment protocol OR state that the study did not involve samples collected from the field.

Ethics oversight

Identify the organization(s) that approved or provided guidance on the study protocol, OR state that no ethical approval or guidance was required and explain why not.

Note that full information on the approval of the study protocol must also be provided in the manuscript.

Clinical data

Policy information about clinical studies

All manuscripts should comply with the ICMJE guidelines for publication of clinical research and a completed CONSORT checklist must be included with all submissions.

Clinical trial registration

Provide the trial registration number from ClinicalTrials.gov or an equivalent agency.

Study protocol

Note where the full trial protocol can be accessed OR if not available, explain why.

Data collection

Describe the settings and locales of data collection, noting the time periods of recruitment and data collection.

Outcomes

Describe how you pre-defined primary and secondary outcome measures and how you assessed these measures.

Dual use research of concern

Policy information about dual use research of concern

Hazards

Could the accidental, deliberate or reckless misuse of agents or technologies generated in the work, or the application of information presented in the manuscript, pose a threat to:

No	Yes	
☒	☐	Public health
☒	☐	National security
☒	☐	Crops and/or livestock
☒	☐	Ecosystems
☒	☐	Any other significant area

Experiments of concern

Does the work involve any of these experiments of concern:

No	Yes	
☒	☐	Demonstrate how to render a vaccine ineffective
☒	☐	Confer resistance to therapeutically useful antibiotics or antiviral agents
☒	☐	Enhance the virulence of a pathogen or render a nonpathogen virulent
☒	☐	Increase transmissibility of a pathogen
☒	☐	Alter the host range of a pathogen
☒	☐	Enable evasion of diagnostic/detection modalities
☒	☐	Enable the weaponization of a biological agent or toxin
☒	☐	Any other potentially harmful combination of experiments and agents

ChIP-seq

Data deposition

☐ Confirm that both raw and final processed data have been deposited in a public database such as GEO.

☐ Confirm that you have deposited or provided access to graph files (e.g. BED files) for the called peaks.

Data access links *May remain private before publication.*	*For "Initial submission" or "Revised version" documents, provide reviewer access links. For your "Final submission" document, provide a link to the deposited data.*
Files in database submission	*Provide a list of all files available in the database submission.*
Genome browser session (e.g. UCSC)	*Provide a link to an anonymized genome browser session for "Initial submission" and "Revised version" documents only, to enable peer review. Write "no longer applicable" for "Final submission" documents.*

Methodology

Replicates	*Describe the experimental replicates, specifying number, type and replicate agreement.*
Sequencing depth	*Describe the sequencing depth for each experiment, providing the total number of reads, uniquely mapped reads, length of reads and whether they were paired- or single-end.*
Antibodies	*Describe the antibodies used for the ChIP-seq experiments; as applicable, provide supplier name, catalog number, clone name, and lot number.*
Peak calling parameters	*Specify the command line program and parameters used for read mapping and peak calling, including the ChIP, control and index files used.*
Data quality	*Describe the methods used to ensure data quality in full detail, including how many peaks are at FDR 5% and above 5-fold enrichment.*
Software	*Describe the software used to collect and analyze the ChIP-seq data. For custom code that has been deposited into a community repository, provide accession details.*

Flow Cytometry

Plots

Confirm that:

☐ The axis labels state the marker and fluorochrome used (e.g. CD4-FITC).

☐ The axis scales are clearly visible. Include numbers along axes only for bottom left plot of group (a 'group' is an analysis of identical markers).

☐ All plots are contour plots with outliers or pseudocolor plots.

☐ A numerical value for number of cells or percentage (with statistics) is provided.

Methodology

Sample preparation	*Describe the sample preparation, detailing the biological source of the cells and any tissue processing steps used.*
Instrument	*Identify the instrument used for data collection, specifying make and model number.*

Software

Describe the software used to collect and analyze the flow cytometry data. For custom code that has been deposited into a community repository, provide accession details.

Cell population abundance

Describe the abundance of the relevant cell populations within post-sort fractions, providing details on the purity of the samples and how it was determined.

Gating strategy

Describe the gating strategy used for all relevant experiments, specifying the preliminary FSC/SSC gates of the starting cell population, indicating where boundaries between "positive" and "negative" staining cell populations are defined.

☐ Tick this box to confirm that a figure exemplifying the gating strategy is provided in the Supplementary Information.

Magnetic resonance imaging

Experimental design

Design type

Indicate task or resting state; event-related or block design.

Design specifications

Specify the number of blocks, trials or experimental units per session and/or subject, and specify the length of each trial or block (if trials are blocked) and interval between trials.

Behavioral performance measures

State number and/or type of variables recorded (e.g. correct button press, response time) and what statistics were used to establish that the subjects were performing the task as expected (e.g. mean, range, and/or standard deviation across subjects).

Acquisition

Imaging type(s)

Specify: functional, structural, diffusion, perfusion.

Field strength

Specify in Tesla

Sequence & imaging parameters

Specify the pulse sequence type (gradient echo, spin echo, etc.), imaging type (EPI, spiral, etc.), field of view, matrix size, slice thickness, orientation and TE/TR/flip angle.

Area of acquisition

State whether a whole brain scan was used OR define the area of acquisition, describing how the region was determined.

Diffusion MRI ☐ Used ☐ Not used

Preprocessing

Preprocessing software

Provide detail on software version and revision number and on specific parameters (model/functions, brain extraction, segmentation, smoothing kernel size, etc.).

Normalization

If data were normalized/standardized, describe the approach(es): specify linear or non-linear and define image types used for transformation OR indicate that data were not normalized and explain rationale for lack of normalization.

Normalization template

Describe the template used for normalization/transformation, specifying subject space or group standardized space (e.g. original Talairach, MNI305, ICBM152) OR indicate that the data were not normalized.

Noise and artifact removal

Describe your procedure(s) for artifact and structured noise removal, specifying motion parameters, tissue signals and physiological signals (heart rate, respiration).

Volume censoring

Define your software and/or method and criteria for volume censoring, and state the extent of such censoring.

Statistical modeling & inference

Model type and settings

Specify type (mass univariate, multivariate, RSA, predictive, etc.) and describe essential details of the model at the first and second levels (e.g. fixed, random or mixed effects; drift or auto-correlation).

Effect(s) tested

Define precise effect in terms of the task or stimulus conditions instead of psychological concepts and indicate whether ANOVA or factorial designs were used.

Specify type of analysis: ☐ Whole brain ☐ ROI-based ☐ Both

Statistic type for inference
(See Eklund et al. 2016)

Specify voxel-wise or cluster-wise and report all relevant parameters for cluster-wise methods.

Correction

Describe the type of correction and how it is obtained for multiple comparisons (e.g. FWE, FDR, permutation or Monte Carlo).

Models & analysis

n/a	Involved in the study
☐	☐ Functional and/or effective connectivity
☐	☐ Graph analysis
☐	☐ Multivariate modeling or predictive analysis

Functional and/or effective connectivity	*Report the measures of dependence used and the model details (e.g. Pearson correlation, partial correlation, mutual information).*
Graph analysis	*Report the dependent variable and connectivity measure, specifying weighted graph or binarized graph, subject- or group-level, and the global and/or node summaries used (e.g. clustering coefficient, efficiency, etc.).*
Multivariate modeling and predictive analysis	*Specify independent variables, features extraction and dimension reduction, model, training and evaluation metrics.*